

# Examining the model dependence of extracting the kinetic freeze-out temperature and transverse flow velocity in small collision system

Hai-Ling Lao<sup>1</sup>, Fu-Hu Liu<sup>1,\*</sup>, Bao-Chun Li<sup>1</sup>, Mai-Ying Duan<sup>1</sup>, Roy A. Lacey<sup>2</sup>

<sup>1</sup>*Institute of Theoretical Physics & State Key Laboratory of Quantum Optics and Quantum Optics Devices, Shanxi University, Taiyuan, Shanxi 030006, China*

<sup>2</sup>*Departments of Chemistry & Physics, Stony Brook University, Stony Brook, NY 11794, USA*

**Abstract:** The kinetic freeze-out temperatures  $T_0$  and transverse flow velocities  $\beta_T$  in small collision systems at high energy are extracted by four variants of the fitting function. The first two variants are the Blast-Wave model with Boltzmann-Gibbs statistics and Tsallis statistics respectively, in which non-zero transverse flow velocity of produced particles is considered. The last two variants are an alternative method which uses the Boltzmann and Tsallis distributions to extract the effective temperatures respectively. Then  $T_0$  and  $\beta_T$  are regarded as the intercept and slope in some linear relations. It is found that the values of  $T_0$  ( $\beta_T$ ) obtained by the four variants are similar, and in some cases the four results are in agreement with each other within errors. In particular, comparing with central nucleus-nucleus collisions, proton-proton collisions are found to be closer to peripheral nucleus-nucleus collisions in terms of  $T_0$  and  $\beta_T$ .

**Keywords:** kinetic freeze-out temperature, transverse flow velocity, small collision system, central nucleus-nucleus collisions, peripheral nucleus-nucleus collisions

**PACS:** 25.75.Ag, 25.75.Dw, 24.10.Pa

## 1 Introduction

As an important concept in both thermal physics and high energy collisions, temperature is widely used in experimental measurements and theoretical studies. Different from macroscopical thermal physics, temperature in microscopical high energy collisions can not be measured directly. Instead, we can obtain the temperature by using the methods of particle ratios and transverse momentum ( $p_T$ ) spectra. The temperature obtained from particle ratios is usually the chemical freeze-out temperature ( $T_{ch}$ ) which describes the excitation degree of the interacting system at the stage of chemical equilibrium. The temperature obtained from  $p_T$  spectra with the thermal distribution which does not include flow effect is usually the effect temperature ( $T_{eff}$  or  $T$ ) which is not a real temperature due to it being related to particle mass. The temperature obtained from  $p_T$  spectra with the thermal distribution which includes flow effect is usually the kinetic freeze-out temperature ( $T_{kin}$  or  $T_0$ ) which describes the excitation degree of the interacting system at the stage of kinetic and thermal equilibrium.

The chemical freeze-out and kinetic freeze-out are two main stages of the interacting system evolution in

high energy collisions. At the stage of chemical freeze-out, the chemical components (relative fractions) of particles are fixed. At the stage of kinetic freeze-out,  $p_T$  and momentum ( $p$ ) spectra of particles are no longer changed. We are interested in  $T_0$  due to its relation to the  $p_T$  spectra of identified particles which are one of the quantities measured in the “first day” in experiments. At the same time,  $T_0$  is related to the structure of phase diagram in the  $T_0$ -related spaces such as  $T_0$ - $\beta_T$  space and  $T_0$ - $\sqrt{s_{NN}}$  space, where  $\beta_T$  denotes the mean transverse flow velocity which is caused by the impact and squeeze,  $\sqrt{s_{NN}}$  denotes the center-of-mass energy per nucleon pair, and  $\sqrt{s_{NN}}$  can be simplified to  $\sqrt{s}$  for proton-proton ( $p$ - $p$  or  $pp$ ) collisions. In particular, in the energy ranges available in the beam energy scan (BES) program at the Relativistic Heavy Ion Collider (RHIC) and the BES program at the Super Proton Synchrotron (SPS), the chemical potential ( $\mu_B$ ) of baryons has to be considered due to its non-negligible value. Then, the structure of phase diagram in  $T_0$ - $\mu_B$  space can be studied in both the RHIC BES and SPS BES energy ranges.

In order to offer facilities for experts who study the structure of phase diagram in the  $T_0$ -related spaces, we have to obtain  $T_0$ ,  $\beta_T$ , and  $\mu_B$  by using reasonable methods firstly. Generally,  $\mu_B$  can be obtained from

\*E-mail: fuhuliu@163.com; fuhuliu@sxu.edu.cn

the particle ratios and its excitation function is studied in detail [1–5], and  $T_0$  and  $\beta_T$  can be obtained from the  $p_T$  spectra. In literature [6–13], different methods on the extractions of  $T_0$  and  $\beta_T$  are used. We are interested in the harmony of different methods. In our recent work [14], we have used a few variants of the fitting function or different methods to extract  $T_0$  and  $\beta_T$  in nucleus-nucleus collisions at the RHIC and Large Hadron Collider (LHC) energies [14–17], where the top RHIC energy is  $\sqrt{s_{NN}} = 200$  GeV and the LHC energy reaches a few and more than ten TeV. The harmonious or similar results are obtained in the case of using non-zero  $\beta_T$  in peripheral nucleus-nucleus collisions in the Blast-Wave model with Boltzmann-Gibbs statistics (the BGBW model) [6–8, 18] and Tsallis statistics (the TBW model) [9, 18, 19]. Our results show that  $T_0$  in central nucleus-nucleus collisions is relatively larger than that in peripheral collisions. Meanwhile,  $T_0$  at the LHC is slightly larger than or nearly equal to that at the RHIC. The situation of  $\beta_T$  is similar to that of  $T_0$ . Comparing with peripheral collisions and the RHIC,  $\beta_T$  shows slightly larger or nearly invariant trend in central collisions and at the LHC.

We are inquisitive to apply the main variants in small collision systems such as  $pp$  and deuteron-gold ( $d$ -Au) collisions at the RHIC, and  $pp$  and proton-lead ( $p$ -Pb) collisions at the LHC, and to show the difference from or similarity to central and peripheral nucleus-nucleus collisions. In this paper, we shall use four variants to extract  $T_0$  and  $\beta_T$  from the  $p_T$  spectra of identified particles produced in  $pp$  and  $d$ -Au collisions at the RHIC, and in  $pp$  and  $p$ -Pb collisions at the LHC. The model results on the  $p_T$  spectra are compared with the experimental data of the PHENIX [20], STAR [21–23], and ALICE Collaborations [24–25], and then  $T_0$  and  $\beta_T$  are extracted from the analyses.

The remainder of this paper is structured as follows. The formalism and method are shortly described in Section 2. Results and discussion are given in Section 3. In Section 4, we summarize our main observations and conclusions.

## 2 Formalism and method

There are four variants or models are used in the present work. The results obtained from the four vari-

ants can be compared with each other. The four variants are:

- i) the BGBW model [6–8] in which non-zero  $\beta_T$  of produced particles is considered by us;
- ii) the TBW model [9] in which non-zero  $\beta_T$  is also considered by us;
- iii) the intercept in  $T - m_0$  relation is regarded as  $T_0$  [7, 10–13], the slope in  $\langle p_T \rangle - \overline{m}$  relation is regarded as  $\beta_T$ , and the slope in  $\langle p \rangle - \overline{m}$  relation is regarded as the radial flow velocity  $\beta$  [14–17] which does not include the contribution of longitudinal flow, where  $m_0$  denotes the rest mass,  $\overline{m}$  denotes the mean moving mass<sup>†</sup>,  $\langle \dots \rangle$  denotes the average on the considered quantity, and  $T$  is obtained by the Boltzmann distribution [18]; and
- iv) in the third variant,  $T$  is obtained by the Tsallis distribution [18, 19].

The four variant can be found in the references mentioned above. In particular, we used the mentioned variants to extract  $T_0$  and  $\beta_T$  in nucleus-nucleus collisions at the RHIC and LHC energies in our recent work [14]. However, to give a whole representation for the present work, we show directly and concisely the four variants in the following.

All of the model descriptions are presented at the mid-rapidity which means that the rapidity  $y \approx 0$  and  $\cosh(y) \approx 1$  which appears in some variants. At the same time, the influences of spin property and chemical potential on the  $p_T$  spectra are neglected due to small effects at the top RHIC and LHC energies. As what we did in our recent work [14], the kinetic freeze-out temperature, the mean transverse (radial) flow velocity, and the effective temperature in different variants are uniformly denoted by  $T_0$ ,  $\beta_T$ , and  $T$ , respectively, though different values can be extracted by different variants.

On the variant i), according to refs. [6–8], the BGBW model results in the  $p_T$  distribution to be

$$f_1(p_T) = \frac{1}{N} \frac{dN}{dp_T} = C_1 p_T m_T \int_0^R r dr \times I_0 \left[ \frac{p_T \sinh(\rho)}{T_0} \right] K_1 \left[ \frac{m_T \cosh(\rho)}{T_0} \right], \quad (1)$$

where  $N$  is the number of particles,  $C_1$  is the normalized constant,  $I_0$  and  $K_1$  are the modified Bessel functions of the first and second kinds respectively,  $m_T = \sqrt{p_T^2 + m_0^2}$  is the transverse mass,  $\rho = \tanh^{-1}[\beta(r)]$  is the boost angle,  $\beta(r) = \beta_S(r/R)^{n_0}$  is a self-similar flow profile,

<sup>†</sup>The mean moving mass is in fact the mean energy  $E$  of the considered particles in the rest frame of source. The momentum  $p$  is obtained by  $p = p_T / \sin \theta$  to obtain  $E$  and  $\beta$  in the rest frame of source, where  $\theta$  is the emission angle and its probability distribution is  $f_\theta(\theta) = \frac{1}{2} \sin \theta$  in the case of considering an isotropic emission in the rest frame of source. However, the multiple sources, if available, distribute mainly along the longitudinal direction, which results strongly in an anisotropic emission and a longitudinal flow which is not the topic studied in the present work. The anisotropic distribution of sources themselves (the anisotropic emission of particles in the center-of mass or laboratory reference frames) and the isotropic emission of particles in the rest frame of source are two different issues.

$\beta_S$  is the flow velocity on the surface,  $r/R$  is the relative radial position in the thermal source, and  $n_0 = 1$  or  $2$  is a free parameter [6]. There is the relation,  $\beta_T = (2/R^2) \int_0^R r \beta(r) dr = 2\beta_S/(n_0 + 2)$ , between  $\beta_T$  and  $\beta(r)$ . In the present work, we take  $n_0 = 2$  as used in ref. [6].

On the variant ii), according to refs. [9], the TBW model results in the  $p_T$  distribution to be

$$f_2(p_T) = \frac{1}{N} \frac{dN}{dp_T} = C_2 p_T m_T \int_{-\pi}^{\pi} d\phi \int_0^R r dr \left\{ 1 + \frac{q-1}{T_0} [m_T \cosh(\rho) - p_T \sinh(\rho) \cos(\phi)] \right\}^{-q/(q-1)}, \quad (2)$$

where  $C_2$  is the normalized constant,  $q$  is an entropy index that characterizes the degree of non-equilibrium,  $\phi$  denotes the azimuth, and  $n_0 = 1$  or  $2$  as used in the BGBW model. In the present work, we take  $n_0 = 1$  as used in ref. [9]. In fact,  $n_0$  is insensitive in the first two variants. It does not matter if we use  $n_0 = 1$  or  $n_0 = 2$ . To be the same as refs. [6] and [9], we use  $n_0 = 2$  in the first variant and  $n_0 = 1$  in the second variant. It should be noted that we use the index  $-q/(q-1)$  in Eq. (2) instead of  $-1/(q-1)$  in ref. [9] due to  $q$  being very close to 1. This substitution results in a small and negligible difference in the Tsallis distribution [19].

As used in our recent work [14], in both the BGBW and TBW models, a non-zero  $\beta_T$  of the produced particles is considered in peripheral nucleus-nucleus collisions. The peripheral collisions contain a few participant nucleons that take part in the violent interactions. This situation is similar to small collision system which also contains a few participant nucleons. In the case of neglecting the influence of cold nuclear effect, small collision system is much similar to peripheral nucleus-nucleus collisions. This means that a non-zero  $\beta_T$  should be considered for small collision system to keep the consistency, though the values of  $\beta_T$  for small collision system and peripheral nucleus-nucleus collisions are possibly different. Naturally, it is not surprised if the values of  $\beta_T$  in the two types of collisions are nearly the same.

The variants iii) and iv) need two steps to obtain  $T_0$  and  $\beta_T$ . To use the relations  $T = T_0 + am_0$ ,  $\langle p_T \rangle = b_1 + \beta_T \overline{m}$ , and  $\langle p \rangle = b_2 + \beta \overline{m}$ , where  $a$ ,  $b_1$ , and  $b_2$  are fitted parameters, we can choose the Boltzmann distribution for the variant iii) and the Tsallis distribution for the variant iv) to fit the  $p_T$  spectra of identified particles produced in high energy collisions. Both the Boltzmann and Tsallis distributions have more than one forms. We choose the form of Boltzmann distribution

[18]

$$f_3(p_T) = \frac{1}{N} \frac{dN}{dp_T} = C_3 p_T m_T \exp\left(-\frac{m_T}{T}\right) \quad (3)$$

and the form of Tsallis distribution [18, 19]

$$f_4(p_T) = \frac{1}{N} \frac{dN}{dp_T} = C_4 p_T m_T \left(1 + \frac{q-1}{T} m_T\right)^{-q/(q-1)}, \quad (4)$$

where  $C_3$  and  $C_4$  are the normalized constants related to the free parameter  $T$ , free parameter  $q$  if it is available, and particle mass  $m_0$  due to its relation to  $m_T$ .

Eqs. (1)–(4) are functions which describe mainly the contribution of soft excitation process. They are only valid for the spectra in a narrow  $p_T$  range which covers 0–2~3 GeV/ $c$  in most cases. Even if for the soft process, the Boltzmann distribution is not enough to fit the  $p_T$  spectra in some cases. In the case of using two- or three-component Boltzmann distribution,  $T$  is the average weighted the effective temperatures and corresponding fractions obtained from different components.

Generally, two main processes in high energy collisions are considered in the present work. Except for the soft excitation process, another main process is the hard scattering process which contributes the spectra in a wide  $p_T$  range and is described by an inverse power-law

$$f_H(p_T) = \frac{1}{N} \frac{dN}{dp_T} = A p_T \left(1 + \frac{p_T}{p_0}\right)^{-n} \quad (5)$$

according to the quantum chromodynamics (QCD) calculus [26–28], where  $p_0$  and  $n$  are free parameters, and  $A$  is the normalized constant related to the free parameters.

The experimental  $p_T$  spectra distribute usually in a wide range. This means that we have to use a superposition of both the contributions of soft and hard processes to fit the spectra. In the present work, the contribution of soft process is described by one of Eqs. (1)–(4), and the contribution of hard process is described by Eq. (5). We have the superposition

$$f_0(p_T) = \frac{1}{N} \frac{dN}{dp_T} = k f_S(p_T) + (1-k) f_H(p_T), \quad (6)$$

where  $k$  denotes the contribution fraction (ratio) of the soft process, and  $f_S(p_T)$  denotes one of Eqs. (1)–(4).

In some cases, in very-low  $p_T$  range, the contributions of resonance production for pions and strong stopping effect for participant nucleons are non-negligible. We have to use a very-soft component for the  $p_T$  range from 0 to 0.2~0.3 GeV/ $c$ . Let  $k_{VS}$  and  $k_S$  denote the

contribution fractions of the very-soft and soft processes respectively. Eq. (6) is revised to be

$$f_0(p_T) = \frac{1}{N} \frac{dN}{dp_T} = k_{VS} f_{VS}(p_T) + k_S f_S(p_T) + (1 - k_{VS} - k_S) f_H(p_T), \quad (7)$$

where  $f_{VS}(p_T)$  denotes one of Eqs. (1)–(4). To keep coordination,  $f_{VS}(p_T)$  is taken to be the same as  $f_S(p_T)$ , but having smaller parameter values. To compare the parameter values obtained from Eqs. (6) and (7), we use the average weighted the parameters and corresponding fractions in very-soft and soft components in Eq. (7). The fraction  $k$  in Eq. (6) corresponds to  $k_{VS} + k_S$  in Eq. (7). In fact, Eq. (6) is a special case of Eq. (7) without the very-soft component.

### 3 Results and discussion

The transverse momentum spectra, in terms of  $1/(2\pi p_T) \cdot d^2N/(dy dp_T)$ , of (a)-(c) positively charged pions ( $\pi^+$ ), positively charged kaons ( $K^+$ ), and protons ( $p$ ), as well as (b)-(d) negatively charged pions ( $\pi^-$ ), negatively charged kaons ( $K^-$ ), and antiprotons ( $\bar{p}$ ) produced in (a)-(b) 0–20% and (c)-(d) 60–88% (40–100%)  $d$ -Au collisions at  $\sqrt{s_{NN}} = 200$  GeV which is the top RHIC energy are presented in Fig. 1, where the spectra for different particles are multiplied by different amounts shown in the panels for the clarity. The closed (open) symbols represent the experimental data of the PHENIX (STAR) Collaboration measured in the pseudorapidity range  $|\eta| < 0.35$  [20] (the rapidity range  $|y| < 0.5$  [21]), where the error bars represent the root quadratic sums of statistical and systematical errors, and the STAR data for  $K^+$  and  $K^-$   $p_T$  spectra are not available. The error bars quoted in this paper are very small. In most cases they disappear within the symbols. The solid, dashed, dotted, and dashed-dotted curves are our results fitted by Eq. (6) or (7) in which  $f_S(p_T)$  ( $f_{VS}(p_T)$ ) denote  $f_1(p_T)$ ,  $f_2(p_T)$ ,  $f_3(p_T)$ , and  $f_4(p_T)$ , respectively. The ratios of data/fit are presented following each panel. The values of parameters  $T_0$ ,  $\beta_T$ ,  $k$ ,  $p_0$ , and  $n$ , normalization constant  $N_0$  which is used to fit the data,  $\chi^2$ , and degree of freedom (dof) (in terms of  $\chi^2/\text{dof}$  for  $\chi^2$  and dof) corresponding to the fit of variant i) are listed in Table 1; the values of  $T_0$ ,  $q$ ,  $\beta_T$ ,  $k$ ,  $p_0$ ,  $n$ ,  $N_0$ ,  $\chi^2$ , and dof corresponding to the variant ii) are listed in Table 2; the values of  $T$ ,  $k$ ,  $p_0$ ,  $n$ ,  $N_0$ ,  $\chi^2$ , and dof corresponding to the variant iii) are listed in Table 3; and the values of  $T$ ,  $q$ ,  $k$ ,  $p_0$ ,  $n$ ,  $N_0$ ,  $\chi^2$ , and dof corresponding to the variant iv) are listed in Table 4. Most of them are fitted by Eq. (6). The numerical values fitted by Eq. (7) are marked by a star at the end of line, in which the results

obtained from the very-soft and soft components are combined. To avoid triviality, the results for very-soft and soft components are not listed particularly. One can see that the four considered variants describe approximately the  $p_T$  spectra of identified particles produced in central (0–20%) and peripheral (60–88% and 40–100%)  $d$ -Au collisions at  $\sqrt{s_{NN}} = 200$  GeV.

Figure 2 is the same as Fig. 1, but it shows the spectra of (a)  $\pi^+$ ,  $K^+$ , and  $p$ , as well as (b)  $\pi^-$ ,  $K^-$ , and  $\bar{p}$ , produced in  $pp$  collisions at  $\sqrt{s} = 200$  GeV. The closed (open) symbols represent the experimental data of the STAR Collaboration measured in  $-0.5 < y < 0$  ( $|y| < 0.5$ ), and the error bars represent the root quadratic sums of statistical and systematical errors [22, 23]. The values of parameters and  $\chi^2/\text{dof}$  corresponding to the fit curves in Fig. 2 are listed in Tables 1–4. One can see that the four considered variants describe approximately the  $p_T$  spectra of identified particles produced in  $pp$  collisions at  $\sqrt{s} = 200$  GeV.

Figure 3 is the same as Fig. 1, but it shows the spectra of  $\pi^+ + \pi^-$ ,  $K^+ + K^-$ , and  $p + \bar{p}$  produced in (a) 0–5% and (b) 80–100%  $p$ -Pb collisions at  $\sqrt{s_{NN}} = 5.02$  TeV which is one of the LHC energies. The symbols represent the experimental data of the ALICE Collaboration measured in  $-0.5 < y < 0$ , and the error bars represent the root quadratic sums of statistical and systematical errors [24]. The values of parameters and  $\chi^2/\text{dof}$  corresponding to the fit curves in Fig. 3 are listed in Tables 1–4, where the results combined the very-soft and soft components are marked by a star at the end of line. One can see that, in most cases, the four considered variants describe approximately the  $p_T$  spectra of identified particles produced in  $p$ -Pb collisions at  $\sqrt{s_{NN}} = 5.02$  TeV.

Figure 4 is the same as Fig. 1, but it shows the spectra, in terms of  $(1/N_{EV}) \cdot 1/(2\pi p_T) \cdot d^2N/(dy dp_T)$ , of  $\pi^+ + \pi^-$ ,  $K^+ + K^-$ , and  $p + \bar{p}$  produced in  $pp$  collisions at  $\sqrt{s} = 2.76$  TeV which is one of the LHC energies, where  $N_{EV}$  denotes the number of events and is usually omitted. The symbols represent the experimental data of the ALICE Collaboration measured in  $|y| < 0.5$  for low- $p_T$  particles and in  $|\eta| < 0.8$  for high- $p_T$  particles, and the error bars represent the root quadratic sums of statistical and systematical errors [25]. The values of parameters and  $\chi^2/\text{dof}$  corresponding to the fit curves in Fig. 4 are listed in Tables 1–4, where the results combined the very-soft and soft components are marked by a star at the end of line. One can see that, in most cases, the four considered variants describe approximately the  $p_T$  spectra of identified particles produced in  $pp$  collisions at  $\sqrt{s} = 2.76$  TeV.

In the fittings in Figs. 1–4, the very-soft component, if available, contributes the  $p_T$  spectra up to 0.2–0.3 GeV/ $c$ . The soft component contributes the  $p_T$  spec-

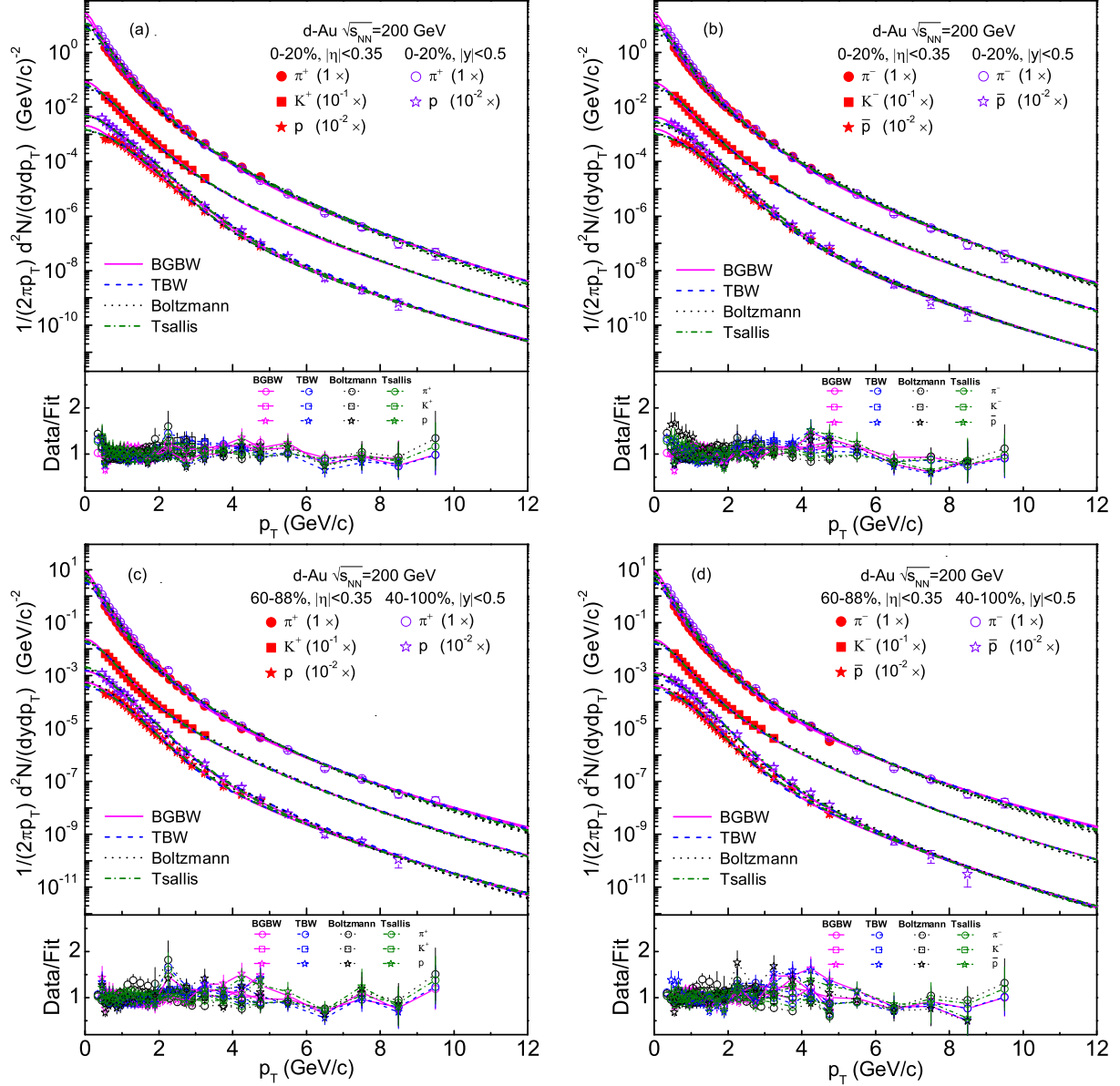


Fig. 1. Transverse momentum spectra of (a)-(c)  $\pi^+$ ,  $K^+$ , and  $p$ , as well as (b)-(d)  $\pi^-$ ,  $K^-$ , and  $\bar{p}$  produced in (a)-(b) 0–20% and (c)-(d) 60–88% (40–100%)  $d$ -Au collisions at  $\sqrt{s_{NN}} = 200$  GeV, where the spectra for different particles are multiplied by different amounts shown in the panels for the clarity. The closed (open) symbols represent the experimental data of the PHENIX (STAR) Collaboration measured in  $|\eta| < 0.35$  [20] ( $|y| < 0.5$  [21]), where the error bars represent the root quadratic sums of statistical and systematical errors, and the STAR data for  $K^+$  and  $K^-$   $p_T$  spectra are not available. In most cases the error bars disappear within the symbols due to their small values. The solid, dashed, dotted, and dashed-dotted curves are our results fitted by Eq. (6) or (7) in which  $f_S(p_T)$  ( $f_{VS}(p_T)$ ) denote  $f_1(p_T)$ ,  $f_2(p_T)$ ,  $f_3(p_T)$ , and  $f_4(p_T)$ , respectively. The ratios of data/fit are presented following each panel.

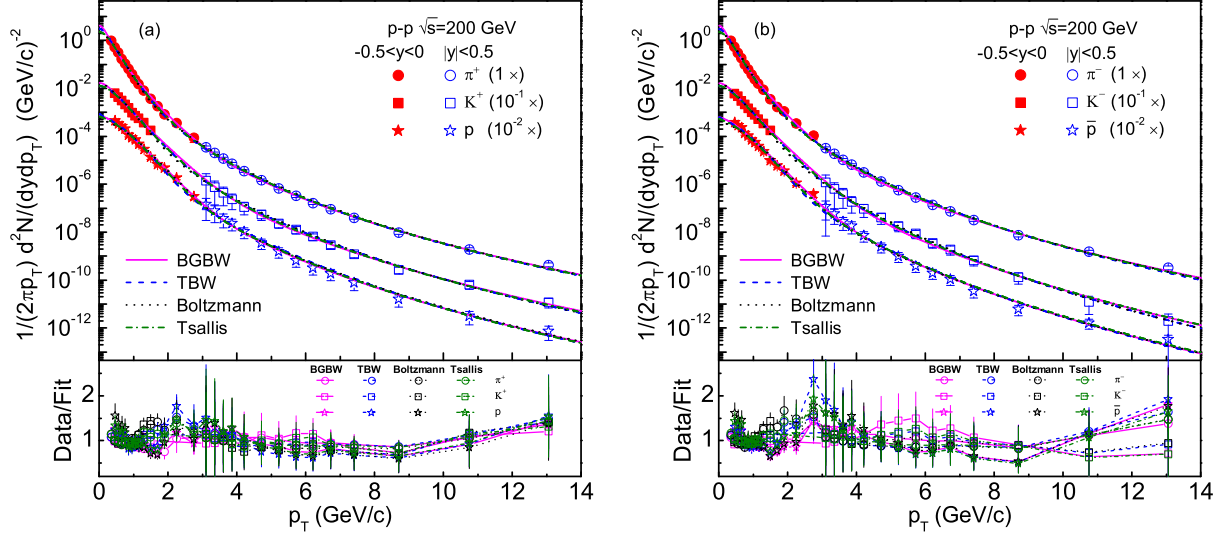


Fig. 2. The same as Fig. 1, but showing the spectra of (a)  $\pi^+$ ,  $K^+$ , and  $p$ , as well as (b)  $\pi^-$ ,  $K^-$ , and  $\bar{p}$ , produced in  $pp$  collisions at  $\sqrt{s} = 200$  GeV. The closed (open) symbols represent the experimental data of the STAR Collaboration measured in  $-0.5 < y < 0$  ( $|y| < 0.5$ ), and the error bars represent the root quadratic sums of statistical and systematical errors [22, 23].

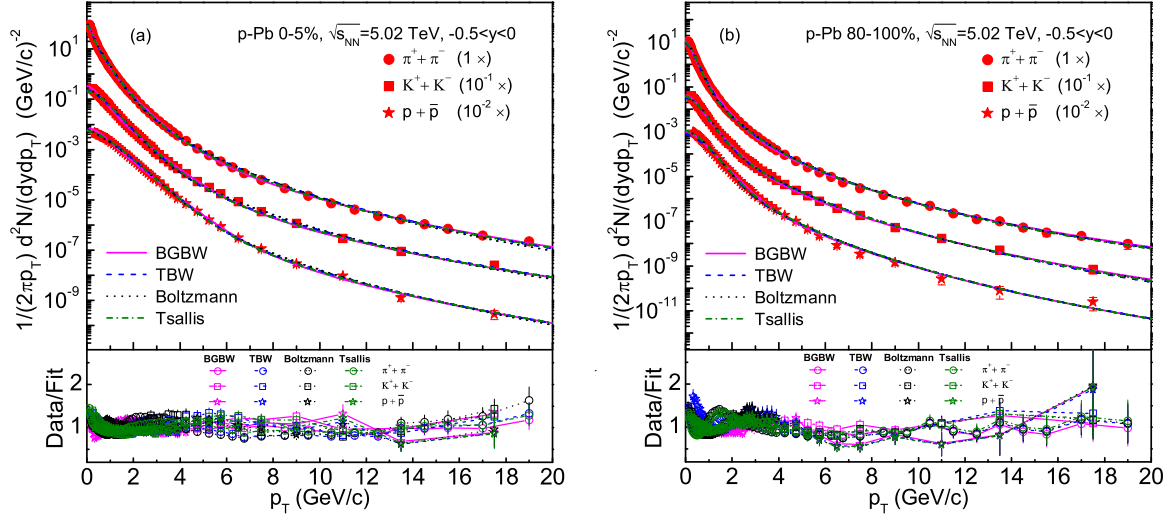


Fig. 3. The same as Fig. 1, but showing the spectra of  $\pi^+ + \pi^-$ ,  $K^+ + K^-$ , and  $p + \bar{p}$  produced in (a) 0–5% and (b) 80–100%  $p$ -Pb collisions at  $\sqrt{s_{NN}} = 5.02$  TeV. The symbols represent the experimental data of the ALICE Collaboration measured in  $-0.5 < y < 0$ , and the error bars represent the root quadratic sums of statistical and systematical errors [24].

tra up to  $2\sim 3$  GeV/ $c$ . However, the hard component contributes the  $p_T$  spectra up to the maximum. In the  $p_T$  range from 0 to  $0.2\sim 0.3$  ( $2\sim 3$ ) GeV/ $c$ , the very-soft (soft) component performs firstly dominating and then obsolescent. At the same time, the soft (hard) component performs firstly as the less important thing and then as the principal one. In the  $p_T$  range from  $0.2\sim 0.3$  ( $2\sim 3$ ) GeV/ $c$  to  $2\sim 3$  GeV/ $c$  (the maximum), the soft (hard) component is the main (sole) contributor. The particular onset  $0.2\sim 0.3$  ( $2\sim 3$ ) GeV/ $c$  of the soft (hard) component as the main (sole) contributor is determined by the least square method which determines the free parameters.

We would like to point out that the root quadratic sums of statistical and systematical errors in the experimental data are used in the above fit process, though the systematical errors are possibly not suitable to be used in some cases. In fact, final errors on the parameters are strongly affected by this choice. Moreover, not all choices are correct (or advisable): as an example, systematic errors on spectra of positive and negative particles are strongly correlated, so counting them in an independent way is not fully correct. It is regretful that if we use only the statistical errors which are very small, the fitting results will be bad. The present work is a preliminary and approximate treatment to obtain the parameters and their errors. As the results, the parameters and their errors contain naturally the effects and contributions of both the statistical and systematical errors in the experimental data.

Although we have used many free parameters in each fit, these parameters are not unrestrictive. In fact, some of them (1–3 parameters) are geared to the very-soft component which describes the very-low  $p_T$  range up to  $0.2\sim 0.3$  GeV/ $c$  in a few cases. Some of them (1–3 parameters) are geared to the soft component which describes the low  $p_T$  range up to  $2\sim 3$  GeV/ $c$  in most cases. While the final two parameters ( $p_0$  and  $n$ ) are geared to the hard component which describes the wide  $p_T$  range up to the maximum. If we use only the narrow  $p_T$  spectra which appear usually in literature, the number of free parameters will be less. However, in this case, the description is incomplete. It is hard to fit the  $p_T$  spectra by using only the very-soft, soft, or hard component. Indeed, we have to use the superposition of the soft and hard components, even including the very-soft component in a few cases. This treatment causes inevitably many free parameters.

The last two variants use the relations between  $T$  and  $m_0$ ,  $\langle p_T \rangle$  and  $\overline{m}$ , as well as  $\langle p \rangle$  and  $\overline{m}$ . They are not suitable to fit simultaneously all particles in low  $p_T$  range due to the mass dependences of the relations. In principle, we can try doing simultaneous fits of all parti-

cles by using the first two variants. In the case of doing simultaneous fits, larger ratio of  $\chi^2/\text{dof}$  will be obtained due to the same set of parameters. Although we fit different particle spectra by different sets of parameters, the mean value of a given parameter can be obtained by weighting different yields of considered particles. The weighted mean parameter is thus regarded as the parameter which is suitable to fit simultaneously all particles. So, both the simultaneous and non-simultaneous fits can be used in analyzing the particle spectra.

Based on the descriptions of  $p_T$  spectra, the first two variants can give  $T_0$  and  $\beta_T$  conveniently, though the values of parameters are possibly not the same due to different variants. To obtain the values of  $T_0$ ,  $\beta_T$ , and  $\beta$  by the variants iii) and iv), we analyze the values of  $T$  presented in Tables 3 and 4, and calculate  $\langle p_T \rangle$ ,  $\langle p \rangle$ , and  $\overline{m}$  based on the values of parameters listed in Tables 3 and 4. In fact, based on an isotropic assumption in the rest frame of emission source and using the Monte Carlo method, we can perform the calculations from  $p_T$  to  $\langle p \rangle$  and  $\overline{m}$  [15–17].

The relations between  $T$  and  $m_0$ ,  $\langle p_T \rangle$  and  $\overline{m}$ , as well as  $\langle p \rangle$  and  $\overline{m}$  are shown in Figs. 5, 6, and 7, respectively, where panels (a) and (b) correspond to the variants iii) and iv) which use the Boltzmann and Tsallis distributions respectively. The symbols in Fig. 5 represent values of  $T$  listed in Tables 3 and 4 for different  $m_0$ . The symbols in Figs. 6 and 7 represent values of  $\langle p_T \rangle$  and  $\langle p \rangle$  for different  $\overline{m}$  respectively, which are calculated due to the parameters listed in Tables 3 and 4 and the isotropic assumption in the rest frame of emission source. The error bars in the three figures are overall errors. The lines in the three figures are the results fitted by the method of least squares for different event samples. The values of intercepts, slopes,  $\chi^2$ , and dof are listed in Tables 5 and 6 which correspond to the variants iii) and iv) respectively. One can see that, in most cases, the mentioned relations are approximately described by linear functions. In particular, the intercept in Fig. 5 reflects  $T_0$ , and the slopes in Figs. 6 and 7 reflect  $\beta_T$  and  $\beta$  respectively. The values of  $T$ ,  $T_0$ ,  $\beta_T$ ,  $\beta$ , and  $\overline{m}$  are approximately independent of isospin.

To compare values of key parameters obtained by different variants for different event samples, Figs. 8 and 9 show the dependences of  $T_0$  and  $\beta_T$  on the centrality  $C$  respectively, where panel (a) corresponds to  $d$ -Au collisions at  $\sqrt{s_{NN}} = 200$  GeV and  $pp$  collisions at  $\sqrt{s} = 200$  GeV, panel (b) corresponds to  $p$ -Pb collisions at  $\sqrt{s_{NN}} = 5.02$  TeV and  $pp$  collisions at  $\sqrt{s} = 2.76$  TeV, and the results for  $pp$  collisions are artificially placed at  $C = 80\%$  for comparison. Different symbols represent the results corresponding to different variants and event samples marked in the panels. The error bars

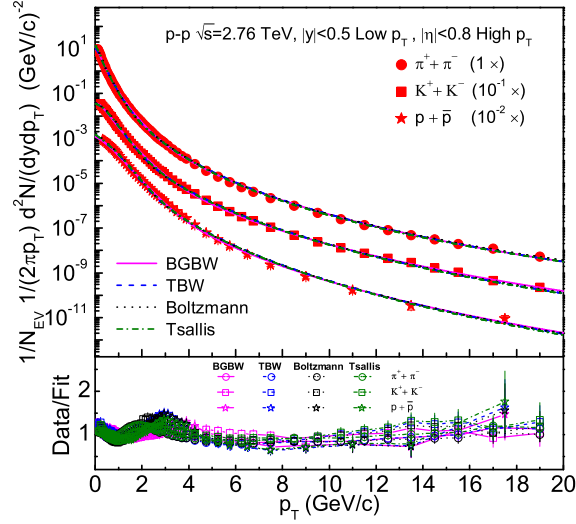


Fig. 4. The same as Fig. 1, but showing the spectra of  $\pi^+ + \pi^-$ ,  $K^+ + K^-$ , and  $p + \bar{p}$  produced in  $pp$  collisions at  $\sqrt{s} = 2.76$  TeV. The symbols represent the experimental data of the ALICE Collaboration measured in  $|y| < 0.5$  for low- $p_T$  particles and in  $|\eta| < 0.8$  for high- $p_T$  particles, and the error bars represent the root quadratic sums of statistical and systematical errors [25].

Table 1. Values of parameters ( $T_0$ ,  $\beta_T$ ,  $k$ ,  $p_0$ , and  $n$ ), normalization constant ( $N_0$ ),  $\chi^2$ , and dof corresponding to the fits of the BGBW model and inverse power-law in Figs. 1–4. The collision types, data sources, and collisions energies are listed in the blank spaces of the first two columns for the purpose of clarity. The results combined the very-soft and soft components are marked by a star (\*) at the end of line.

Figure	Centrality	Particle	$T_0$ (GeV)	$\beta_T$ (c)	$k$	$p_0$ (GeV/c)	$n$	$N_0$	$\chi^2/\text{dof}$
1(a)	0–20%	$\pi^+$	$0.109 \pm 0.006$	$0.423 \pm 0.011$	$0.940 \pm 0.011$	$5.226 \pm 0.286$	$15.597 \pm 0.361$	$22.424 \pm 1.933$	14.130/18
PHENIX	200 GeV	$K^+$	$0.124 \pm 0.008$	$0.412 \pm 0.010$	$0.890 \pm 0.012$	$6.294 \pm 0.295$	$15.609 \pm 0.398$	$1.070 \pm 0.087$	5.010/15
		$p$	$0.129 \pm 0.008$	$0.387 \pm 0.008$	$0.901 \pm 0.010$	$5.675 \pm 0.251$	$14.288 \pm 0.375$	$0.275 \pm 0.023$	55.314/18
1(b)	0–20%	$\pi^-$	$0.109 \pm 0.006$	$0.423 \pm 0.011$	$0.940 \pm 0.011$	$5.746 \pm 0.272$	$16.657 \pm 0.373$	$21.805 \pm 1.995$	8.946/18
		$K^-$	$0.124 \pm 0.008$	$0.412 \pm 0.010$	$0.890 \pm 0.012$	$6.404 \pm 0.288$	$15.998 \pm 0.383$	$0.996 \pm 0.095$	3.960/15
		$\bar{p}$	$0.128 \pm 0.008$	$0.387 \pm 0.008$	$0.901 \pm 0.010$	$5.675 \pm 0.232$	$14.908 \pm 0.358$	$0.209 \pm 0.017$	66.132/18
1(c)	60–88%	$\pi^+$	$0.103 \pm 0.006$	$0.415 \pm 0.011$	$0.955 \pm 0.010$	$3.797 \pm 0.151$	$12.582 \pm 0.286$	$6.949 \pm 0.630$	12.060/18
		$K^+$	$0.114 \pm 0.008$	$0.395 \pm 0.010$	$0.879 \pm 0.012$	$6.889 \pm 0.212$	$16.194 \pm 0.291$	$0.304 \pm 0.032$	12.075/15
		$p$	$0.119 \pm 0.009$	$0.365 \pm 0.009$	$0.916 \pm 0.013$	$5.939 \pm 0.198$	$14.633 \pm 0.232$	$0.075 \pm 0.007$	27.486/18
1(d)	60–88%	$\pi^-$	$0.103 \pm 0.006$	$0.415 \pm 0.011$	$0.955 \pm 0.010$	$3.797 \pm 0.151$	$12.522 \pm 0.281$	$6.771 \pm 0.630$	11.070/18
		$K^-$	$0.113 \pm 0.008$	$0.392 \pm 0.011$	$0.879 \pm 0.012$	$6.889 \pm 0.212$	$16.508 \pm 0.297$	$0.290 \pm 0.026$	7.050/15
		$\bar{p}$	$0.117 \pm 0.008$	$0.367 \pm 0.009$	$0.916 \pm 0.013$	$5.939 \pm 0.198$	$15.466 \pm 0.288$	$0.056 \pm 0.007$	29.628/18
1(a)	0–20%	$\pi^+$	$0.108 \pm 0.006$	$0.422 \pm 0.011$	$0.958 \pm 0.010$	$4.576 \pm 0.223$	$14.491 \pm 0.328$	$32.525 \pm 2.793$	13.950/18
$d$ -Au	200 GeV	$p$	$0.127 \pm 0.008$	$0.371 \pm 0.008$	$0.933 \pm 0.008$	$6.075 \pm 0.239$	$15.525 \pm 0.349$	$0.704 \pm 0.064$	15.936/16
1(b)	0–20%	$\pi^-$	$0.108 \pm 0.006$	$0.422 \pm 0.011$	$0.958 \pm 0.010$	$4.656 \pm 0.231$	$14.765 \pm 0.332$	$32.970 \pm 2.816$	12.114/18
STAR		$\bar{p}$	$0.126 \pm 0.005$	$0.368 \pm 0.008$	$0.936 \pm 0.007$	$6.065 \pm 0.108$	$16.038 \pm 0.178$	$0.587 \pm 0.047$	22.640/16
1(c)	40–100%	$\pi^+$	$0.102 \pm 0.006$	$0.415 \pm 0.010$	$0.956 \pm 0.009$	$3.697 \pm 0.176$	$12.783 \pm 0.288$	$10.286 \pm 0.761$	17.352/18
		$p$	$0.115 \pm 0.007$	$0.365 \pm 0.007$	$0.950 \pm 0.008$	$6.928 \pm 0.149$	$16.683 \pm 0.302$	$0.199 \pm 0.016$	27.936/16
		$\pi^-$	$0.102 \pm 0.006$	$0.415 \pm 0.010$	$0.963 \pm 0.009$	$3.697 \pm 0.176$	$12.283 \pm 0.279$	$10.539 \pm 0.782$	14.544/18
1(d)	40–100%	$\bar{p}$	$0.113 \pm 0.006$	$0.361 \pm 0.007$	$0.952 \pm 0.008$	$6.858 \pm 0.145$	$17.606 \pm 0.311$	$0.164 \pm 0.014$	37.296/16
2(a)		$\pi^+$	$0.103 \pm 0.006$	$0.401 \pm 0.011$	$0.946 \pm 0.010$	$2.435 \pm 0.103$	$10.856 \pm 0.298$	$5.078 \pm 0.579$	35.098/23
$pp$	200 GeV	$K^+$	$0.112 \pm 0.008$	$0.401 \pm 0.011$	$0.934 \pm 0.012$	$3.218 \pm 0.142$	$11.667 \pm 0.316$	$0.222 \pm 0.027$	7.974/18
		$p$	$0.115 \pm 0.008$	$0.341 \pm 0.009$	$0.863 \pm 0.014$	$3.262 \pm 0.151$	$12.398 \pm 0.342$	$0.096 \pm 0.010$	25.476/22
2(b)		$\pi^-$	$0.103 \pm 0.006$	$0.401 \pm 0.011$	$0.945 \pm 0.010$	$2.338 \pm 0.106$	$10.859 \pm 0.298$	$5.074 \pm 0.575$	37.490/23
		$K^-$	$0.112 \pm 0.008$	$0.401 \pm 0.011$	$0.958 \pm 0.012$	$3.997 \pm 0.148$	$13.538 \pm 0.328$	$0.218 \pm 0.027$	7.380/18
		$\bar{p}$	$0.115 \pm 0.008$	$0.341 \pm 0.009$	$0.860 \pm 0.014$	$3.662 \pm 0.165$	$13.722 \pm 0.351$	$0.081 \pm 0.010$	49.148/22
3(a)	0–5%	$\pi^\pm$	$0.137 \pm 0.008$	$0.428 \pm 0.012$	$0.930 \pm 0.011$	$2.240 \pm 0.106$	$7.383 \pm 0.289$	$97.136 \pm 9.684$	164.008/49*
$p$ -Pb	5.02 TeV	$K^\pm$	$0.189 \pm 0.009$	$0.428 \pm 0.011$	$0.927 \pm 0.012$	$2.849 \pm 0.113$	$7.189 \pm 0.296$	$3.986 \pm 0.412$	51.390/45
		$p+\bar{p}$	$0.193 \pm 0.009$	$0.417 \pm 0.011$	$0.936 \pm 0.011$	$3.588 \pm 0.165$	$8.345 \pm 0.312$	$0.943 \pm 0.102$	185.975/43
3(b)	80–100%	$\pi^\pm$	$0.110 \pm 0.008$	$0.412 \pm 0.011$	$0.880 \pm 0.012$	$1.625 \pm 0.101$	$7.228 \pm 0.292$	$12.446 \pm 1.171$	201.240/52
		$K^\pm$	$0.138 \pm 0.008$	$0.398 \pm 0.010$	$0.898 \pm 0.011$	$3.455 \pm 0.135$	$8.572 \pm 0.301$	$0.541 \pm 0.060$	66.510/45
		$p+\bar{p}$	$0.153 \pm 0.009$	$0.354 \pm 0.010$	$0.886 \pm 0.012$	$4.012 \pm 0.144$	$9.697 \pm 0.310$	$0.129 \pm 0.016$	167.356/43
4		$\pi^\pm$	$0.109 \pm 0.008$	$0.417 \pm 0.011$	$0.888 \pm 0.012$	$2.014 \pm 0.108$	$8.008 \pm 0.298$	$11.181 \pm 1.195$	212.895/57
$pp$	2.76 TeV	$K^\pm$	$0.140 \pm 0.008$	$0.403 \pm 0.010$	$0.890 \pm 0.010$	$2.995 \pm 0.132$	$8.382 \pm 0.306$	$0.473 \pm 0.055$	51.168/52
		$p+\bar{p}$	$0.148 \pm 0.009$	$0.353 \pm 0.010$	$0.801 \pm 0.012$	$2.832 \pm 0.126$	$9.177 \pm 0.302$	$0.140 \pm 0.017$	127.538/43



Table 2. The same as Table 1, but showing the values of parameters ( $T_0$ ,  $q$ ,  $\beta_T$ ,  $k$ ,  $p_0$ , and  $n$ ), normalization constant ( $N_0$ ),  $\chi^2$ , and dof corresponding to the fits of the TBW model and inverse power-law in Figs. 1–4.

Figure	Centrality	Particle	$T_0$ (GeV)	$q$	$\beta_T$ (c)	$k$	$p_0$ (GeV/c)	$n$	$N_0$	$\chi^2/\text{dof}$	
1(a) d-Au PHENIX	0–20%	$\pi^+$	$0.106 \pm 0.006$	$1.020 \pm 0.007$	$0.442 \pm 0.012$	$0.895 \pm 0.012$	$5.219 \pm 0.258$	$15.896 \pm 0.386$	$10.858 \pm 1.050$	$37.825/17$	
		$K^+$	$0.116 \pm 0.008$	$1.022 \pm 0.008$	$0.442 \pm 0.012$	$0.814 \pm 0.011$	$6.166 \pm 0.288$	$15.955 \pm 0.392$	$0.750 \pm 0.067$	$12.796/14$	
		$p$	$0.118 \pm 0.008$	$1.018 \pm 0.007$	$0.439 \pm 0.010$	$0.889 \pm 0.011$	$5.675 \pm 0.249$	$14.383 \pm 0.382$	$0.188 \pm 0.016$	$23.103/17$	
	0–20%	$\pi^-$	$0.106 \pm 0.006$	$1.020 \pm 0.007$	$0.445 \pm 0.012$	$0.896 \pm 0.012$	$5.601 \pm 0.260$	$16.750 \pm 0.389$	$10.730 \pm 1.033$	$35.224/17$	
		$K^-$	$0.116 \pm 0.008$	$1.022 \pm 0.008$	$0.442 \pm 0.012$	$0.858 \pm 0.010$	$6.324 \pm 0.290$	$16.115 \pm 0.383$	$0.752 \pm 0.067$	$20.006/14$	
		$\bar{p}$	$0.117 \pm 0.008$	$1.018 \pm 0.007$	$0.439 \pm 0.010$	$0.880 \pm 0.010$	$5.598 \pm 0.243$	$14.953 \pm 0.386$	$0.138 \pm 0.010$	$28.662/17$	
1(c)	60–88%	$\pi^+$	$0.085 \pm 0.006$	$1.039 \pm 0.008$	$0.453 \pm 0.011$	$0.911 \pm 0.012$	$3.657 \pm 0.186$	$12.782 \pm 0.346$	$3.958 \pm 0.381$	$13.566/17$	
		$K^+$	$0.090 \pm 0.008$	$1.029 \pm 0.008$	$0.445 \pm 0.012$	$0.843 \pm 0.013$	$6.824 \pm 0.292$	$16.294 \pm 0.386$	$0.220 \pm 0.023$	$12.558/14$	
		$p$	$0.097 \pm 0.008$	$1.012 \pm 0.007$	$0.433 \pm 0.011$	$0.892 \pm 0.011$	$5.839 \pm 0.201$	$14.633 \pm 0.232$	$0.052 \pm 0.006$	$20.978/17$	
1(d)	60–88%	$\pi^-$	$0.085 \pm 0.006$	$1.039 \pm 0.008$	$0.453 \pm 0.011$	$0.911 \pm 0.012$	$3.517 \pm 0.182$	$12.522 \pm 0.328$	$4.002 \pm 0.237$	$21.692/17$	
		$K^-$	$0.090 \pm 0.008$	$1.028 \pm 0.008$	$0.445 \pm 0.012$	$0.843 \pm 0.013$	$6.722 \pm 0.283$	$16.508 \pm 0.388$	$0.211 \pm 0.021$	$12.796/14$	
		$\bar{p}$	$0.096 \pm 0.008$	$1.011 \pm 0.007$	$0.436 \pm 0.011$	$0.885 \pm 0.011$	$5.724 \pm 0.211$	$15.466 \pm 0.265$	$0.041 \pm 0.006$	$30.957/17$	
1(a) d-Au STAR	0–20%	$\pi^+$	$0.104 \pm 0.006$	$1.020 \pm 0.008$	$0.449 \pm 0.012$	$0.913 \pm 0.012$	$4.396 \pm 0.188$	$14.655 \pm 0.386$	$13.969 \pm 1.394$	$33.864/17$	
		$p$	$0.114 \pm 0.008$	$1.010 \pm 0.007$	$0.400 \pm 0.010$	$0.899 \pm 0.011$	$6.018 \pm 0.203$	$15.831 \pm 0.378$	$0.657 \pm 0.047$	$23.187/11^*$	
		$\pi^-$	$0.104 \pm 0.006$	$1.020 \pm 0.008$	$0.449 \pm 0.012$	$0.913 \pm 0.012$	$4.466 \pm 0.192$	$14.885 \pm 0.388$	$13.973 \pm 1.395$	$33.065/17$	
	40–100%	$\bar{p}$	$0.116 \pm 0.008$	$1.008 \pm 0.005$	$0.430 \pm 0.010$	$0.891 \pm 0.011$	$5.773 \pm 0.167$	$16.118 \pm 0.384$	$0.415 \pm 0.036$	$38.175/15$	
		$\pi^+$	$0.083 \pm 0.006$	$1.038 \pm 0.008$	$0.445 \pm 0.012$	$0.921 \pm 0.012$	$3.436 \pm 0.158$	$12.783 \pm 0.316$	$7.069 \pm 0.689$	$22.559/17$	
		$p$	$0.091 \pm 0.008$	$1.014 \pm 0.007$	$0.383 \pm 0.010$	$0.912 \pm 0.011$	$6.418 \pm 0.215$	$16.683 \pm 0.368$	$0.213 \pm 0.009$	$26.024/11^*$	
1(d)	40–100%	$\pi^-$	$0.083 \pm 0.006$	$1.038 \pm 0.008$	$0.445 \pm 0.012$	$0.929 \pm 0.011$	$3.432 \pm 0.156$	$12.632 \pm 0.308$	$7.081 \pm 0.690$	$20.468/17$	
		$\bar{p}$	$0.094 \pm 0.008$	$1.016 \pm 0.007$	$0.432 \pm 0.010$	$0.908 \pm 0.011$	$5.559 \pm 0.188$	$16.113 \pm 0.326$	$0.113 \pm 0.008$	$55.395/15$	
		2(a) pp STAR	200 GeV	$\pi^+$	$0.086 \pm 0.006$	$1.017 \pm 0.008$	$0.421 \pm 0.013$	$0.877 \pm 0.014$	$2.135 \pm 0.139$	$10.786 \pm 0.339$	$3.926 \pm 0.416$
$K^+$	$0.097 \pm 0.008$			$1.028 \pm 0.009$	$0.421 \pm 0.013$	$0.886 \pm 0.014$	$3.523 \pm 0.159$	$12.598 \pm 0.356$	$0.171 \pm 0.025$	$15.164/17$	
$p$	$0.103 \pm 0.009$			$1.002 \pm 0.001$	$0.371 \pm 0.010$	$0.762 \pm 0.012$	$3.262 \pm 0.166$	$12.846 \pm 0.355$	$0.100 \pm 0.015$	$29.421/21$	
2(b)			$\pi^-$	$0.086 \pm 0.006$	$1.017 \pm 0.008$	$0.421 \pm 0.013$	$0.837 \pm 0.014$	$2.204 \pm 0.137$	$11.286 \pm 0.332$	$3.819 \pm 0.425$	$27.874/22$
			$K^-$	$0.097 \pm 0.008$	$1.028 \pm 0.009$	$0.421 \pm 0.013$	$0.883 \pm 0.014$	$3.963 \pm 0.162$	$14.386 \pm 0.365$	$0.169 \pm 0.022$	$7.378/17$
			$\bar{p}$	$0.104 \pm 0.009$	$1.002 \pm 0.001$	$0.376 \pm 0.010$	$0.802 \pm 0.011$	$3.602 \pm 0.201$	$13.882 \pm 0.362$	$0.075 \pm 0.012$	$40.068/21$
3(a) p-Pb ALICE	0–5%	$\pi^\pm$	$0.099 \pm 0.007$	$1.002 \pm 0.001$	$0.486 \pm 0.013$	$0.785 \pm 0.013$	$2.005 \pm 0.118$	$7.729 \pm 0.296$	$98.948 \pm 10.934$	$323.312/47^*$	
		$K^\pm$	$0.184 \pm 0.009$	$1.012 \pm 0.006$	$0.462 \pm 0.012$	$0.890 \pm 0.012$	$2.959 \pm 0.163$	$7.499 \pm 0.284$	$2.892 \pm 0.330$	$200.992/44$	
		$p+\bar{p}$	$0.196 \pm 0.009$	$1.015 \pm 0.008$	$0.460 \pm 0.012$	$0.875 \pm 0.012$	$3.388 \pm 0.198$	$8.585 \pm 0.321$	$0.723 \pm 0.083$	$57.204/42$	
	3(b)	80–100%	$\pi^\pm$	$0.088 \pm 0.006$	$1.002 \pm 0.001$	$0.453 \pm 0.011$	$0.762 \pm 0.013$	$1.445 \pm 0.109$	$7.328 \pm 0.298$	$11.396 \pm 1.228$	$484.449/51$
			$K^\pm$	$0.110 \pm 0.008$	$1.011 \pm 0.006$	$0.448 \pm 0.011$	$0.841 \pm 0.012$	$3.805 \pm 0.196$	$9.302 \pm 0.323$	$0.447 \pm 0.054$	$208.384/44$
			$p+\bar{p}$	$0.112 \pm 0.009$	$1.001 \pm 0.001$	$0.442 \pm 0.010$	$0.781 \pm 0.013$	$3.442 \pm 0.181$	$9.427 \pm 0.331$	$0.102 \pm 0.011$	$416.052/42$
4 pp ALICE	2.76 TeV	$\pi^\pm$	$0.086 \pm 0.006$	$1.002 \pm 0.001$	$0.453 \pm 0.011$	$0.784 \pm 0.012$	$1.665 \pm 0.108$	$7.846 \pm 0.302$	$11.808 \pm 1.047$	$290.960/52^*$	
		$K^\pm$	$0.110 \pm 0.008$	$1.009 \pm 0.006$	$0.453 \pm 0.011$	$0.771 \pm 0.013$	$2.765 \pm 0.146$	$8.692 \pm 0.321$	$0.455 \pm 0.056$	$146.319/51$	
		$p+\bar{p}$	$0.113 \pm 0.008$	$1.001 \pm 0.001$	$0.420 \pm 0.010$	$0.603 \pm 0.012$	$2.592 \pm 0.157$	$9.348 \pm 0.332$	$0.168 \pm 0.018$	$273.504/42$	

Table 3. The same as Table 1, but showing the values of parameters ( $T$ ,  $k$ ,  $p_0$ , and  $n$ ), normalization constant ( $N_0$ ),  $\chi^2$ , and dof corresponding to the fits of the Boltzmann distribution and inverse power-law in Figs. 1–4.

Figure	Centrality	Particle	$T$ (GeV)	$k$	$p_0$ (GeV/c)	$n$	$N_0$	$\chi^2/\text{dof}$
1(a)	0–20%	$\pi^+$	$0.172 \pm 0.006$	$0.765 \pm 0.013$	$4.766 \pm 0.166$	$15.886 \pm 0.321$	$7.635 \pm 0.720$	$35.473/19$
$d$ -Au	200 GeV	$K^+$	$0.231 \pm 0.009$	$0.761 \pm 0.014$	$6.034 \pm 0.215$	$15.932 \pm 0.342$	$0.655 \pm 0.067$	$22.000/16$
PHENIX		$p$	$0.290 \pm 0.009$	$0.878 \pm 0.014$	$5.975 \pm 0.198$	$14.935 \pm 0.316$	$0.187 \pm 0.018$	$19.722/19$
1(b)	0–20%	$\pi^-$	$0.172 \pm 0.006$	$0.742 \pm 0.013$	$5.161 \pm 0.183$	$16.855 \pm 0.365$	$6.919 \pm 0.698$	$30.666/19$
		$K^-$	$0.231 \pm 0.009$	$0.763 \pm 0.014$	$6.504 \pm 0.206$	$16.868 \pm 0.338$	$0.626 \pm 0.060$	$17.216/16$
		$\bar{p}$	$0.286 \pm 0.009$	$0.856 \pm 0.014$	$5.863 \pm 0.176$	$15.558 \pm 0.348$	$0.150 \pm 0.013$	$31.445/19$
1(c)	60–88%	$\pi^+$	$0.137 \pm 0.006$	$0.655 \pm 0.013$	$3.006 \pm 0.113$	$12.935 \pm 0.236$	$3.474 \pm 0.339$	$42.009/19$
		$K^+$	$0.185 \pm 0.009$	$0.762 \pm 0.014$	$6.667 \pm 0.226$	$16.848 \pm 0.329$	$0.239 \pm 0.024$	$5.280/16$
		$p$	$0.211 \pm 0.009$	$0.728 \pm 0.014$	$5.129 \pm 0.206$	$15.113 \pm 0.298$	$0.089 \pm 0.009$	$50.540/19$
1(d)	60–88%	$\pi^-$	$0.137 \pm 0.006$	$0.655 \pm 0.013$	$3.006 \pm 0.113$	$12.935 \pm 0.236$	$3.451 \pm 0.332$	$64.980/19$
		$K^-$	$0.185 \pm 0.009$	$0.762 \pm 0.014$	$6.408 \pm 0.216$	$16.848 \pm 0.329$	$0.238 \pm 0.029$	$10.272/16$
		$\bar{p}$	$0.211 \pm 0.009$	$0.735 \pm 0.014$	$4.889 \pm 0.188$	$15.323 \pm 0.296$	$0.070 \pm 0.007$	$54.644/19$
1(a)	0–20%	$\pi^+$	$0.170 \pm 0.007$	$0.786 \pm 0.013$	$4.236 \pm 0.148$	$15.461 \pm 0.263$	$11.493 \pm 1.231$	$36.119/19$
$d$ -Au	200 GeV	$p$	$0.251 \pm 0.009$	$0.912 \pm 0.014$	$5.885 \pm 0.166$	$15.525 \pm 0.298$	$0.633 \pm 0.047$	$24.542/15^*$
1(b)	0–20%	$\pi^-$	$0.170 \pm 0.007$	$0.786 \pm 0.013$	$4.236 \pm 0.148$	$15.461 \pm 0.263$	$11.493 \pm 1.231$	$35.226/19$
STAR		$\bar{p}$	$0.283 \pm 0.008$	$0.878 \pm 0.013$	$5.355 \pm 0.156$	$15.345 \pm 0.287$	$0.325 \pm 0.035$	$57.358/17$
1(c)	40–100%	$\pi^+$	$0.138 \pm 0.007$	$0.781 \pm 0.014$	$2.777 \pm 0.089$	$12.433 \pm 0.216$	$5.920 \pm 0.579$	$45.182/19$
		$p$	$0.209 \pm 0.009$	$0.788 \pm 0.014$	$4.868 \pm 0.153$	$15.426 \pm 0.268$	$0.236 \pm 0.023$	$25.959/17$
1(d)	40–100%	$\pi^-$	$0.138 \pm 0.007$	$0.781 \pm 0.014$	$2.777 \pm 0.089$	$12.433 \pm 0.216$	$5.920 \pm 0.579$	$37.449/19$
		$\bar{p}$	$0.210 \pm 0.009$	$0.784 \pm 0.013$	$4.585 \pm 0.146$	$15.456 \pm 0.275$	$0.188 \pm 0.016$	$33.558/17$
2(a)		$\pi^+$	$0.138 \pm 0.007$	$0.766 \pm 0.013$	$1.908 \pm 0.130$	$10.596 \pm 0.285$	$2.931 \pm 0.334$	$44.880/24$
$pp$	200 GeV	$K^+$	$0.180 \pm 0.009$	$0.651 \pm 0.014$	$2.583 \pm 0.145$	$11.735 \pm 0.299$	$0.233 \pm 0.025$	$24.510/19$
STAR		$p$	$0.223 \pm 0.009$	$0.868 \pm 0.014$	$3.672 \pm 0.168$	$12.934 \pm 0.264$	$0.069 \pm 0.009$	$41.170/23$
2(b)		$\pi^-$	$0.140 \pm 0.008$	$0.758 \pm 0.013$	$1.908 \pm 0.132$	$10.809 \pm 0.249$	$2.989 \pm 0.333$	$47.568/24$
		$K^-$	$0.180 \pm 0.009$	$0.651 \pm 0.014$	$3.118 \pm 0.142$	$13.665 \pm 0.286$	$0.226 \pm 0.028$	$14.041/19$
		$\bar{p}$	$0.223 \pm 0.009$	$0.860 \pm 0.014$	$3.735 \pm 0.165$	$13.698 \pm 0.309$	$0.056 \pm 0.009$	$54.119/23$
3(a)	0–5%	$\pi^\pm$	$0.160 \pm 0.008$	$0.692 \pm 0.014$	$2.005 \pm 0.116$	$8.016 \pm 0.282$	$96.519 \pm 11.020$	$375.602/51^*$
$p$ -Pb	5.02 TeV	$K^\pm$	$0.310 \pm 0.008$	$0.726 \pm 0.015$	$2.603 \pm 0.126$	$7.813 \pm 0.296$	$3.345 \pm 0.356$	$201.204/46$
ALICE		$p+\bar{p}$	$0.421 \pm 0.009$	$0.725 \pm 0.015$	$3.275 \pm 0.143$	$8.989 \pm 0.302$	$0.764 \pm 0.098$	$95.920/44$
3(b)	80–100%	$\pi^\pm$	$0.125 \pm 0.009$	$0.690 \pm 0.015$	$1.345 \pm 0.098$	$7.298 \pm 0.288$	$10.991 \pm 1.250$	$655.981/53$
		$K^\pm$	$0.210 \pm 0.010$	$0.788 \pm 0.015$	$2.903 \pm 0.115$	$8.506 \pm 0.291$	$0.473 \pm 0.069$	$260.222/46$
		$p+\bar{p}$	$0.232 \pm 0.010$	$0.806 \pm 0.013$	$3.532 \pm 0.146$	$9.587 \pm 0.299$	$0.140 \pm 0.017$	$168.168/44$
4		$\pi^\pm$	$0.119 \pm 0.008$	$0.602 \pm 0.015$	$1.225 \pm 0.094$	$7.398 \pm 0.272$	$14.229 \pm 2.048$	$232.037/56^*$
$pp$	2.76 TeV	$K^\pm$	$0.208 \pm 0.009$	$0.765 \pm 0.015$	$2.595 \pm 0.105$	$8.488 \pm 0.296$	$0.469 \pm 0.065$	$229.914/53$
ALICE		$p+\bar{p}$	$0.238 \pm 0.009$	$0.645 \pm 0.012$	$2.512 \pm 0.103$	$9.203 \pm 0.302$	$0.182 \pm 0.016$	$214.192/44$

Table 4. The same as Table 1, but showing the values of parameters ( $T$ ,  $q$ ,  $k$ ,  $p_0$ , and  $n$ ), normalization constant ( $N_0$ ),  $\chi^2$ , and dof corresponding to the fits of the Tsallis distribution and inverse power-law in Figs. 1–4.

Figure	Centrality	Particle	$T$ (GeV)	$q$	$k$	$p_0$ (GeV/c)	$n$	$N_0$	$\chi^2/\text{dof}$
1(a)	0–20%	$\pi^+$	$0.130 \pm 0.008$	$1.071 \pm 0.009$	$0.875 \pm 0.015$	$4.923 \pm 0.189$	$15.557 \pm 0.365$	$9.879 \pm 1.113$	7.8480/18
PHENIX 1(b)	200 GeV	$K^+$	$0.182 \pm 0.009$	$1.042 \pm 0.010$	$0.802 \pm 0.016$	$6.294 \pm 0.213$	$16.342 \pm 0.388$	$0.840 \pm 0.086$	10.530/15
		$p$	$0.267 \pm 0.009$	$1.015 \pm 0.007$	$0.878 \pm 0.011$	$5.675 \pm 0.218$	$14.535 \pm 0.368$	$0.195 \pm 0.022$	18.144/18
		$\pi^-$	$0.130 \pm 0.008$	$1.071 \pm 0.009$	$0.875 \pm 0.015$	$4.923 \pm 0.189$	$15.787 \pm 0.368$	$9.896 \pm 1.115$	15.822/18
1(c)	60–88%	$K^-$	$0.182 \pm 0.009$	$1.042 \pm 0.010$	$0.802 \pm 0.016$	$6.144 \pm 0.205$	$16.342 \pm 0.388$	$0.799 \pm 0.081$	10.140/15
		$\bar{p}$	$0.268 \pm 0.009$	$1.015 \pm 0.007$	$0.876 \pm 0.012$	$5.875 \pm 0.226$	$15.298 \pm 0.374$	$0.138 \pm 0.020$	32.868/18
		$\pi^+$	$0.104 \pm 0.008$	$1.082 \pm 0.009$	$0.919 \pm 0.015$	$3.627 \pm 0.148$	$12.912 \pm 0.315$	$5.028 \pm 0.549$	17.874/18
1(d)	60–88%	$K^+$	$0.136 \pm 0.009$	$1.072 \pm 0.011$	$0.872 \pm 0.016$	$6.679 \pm 0.248$	$15.998 \pm 0.395$	$0.251 \pm 0.027$	6.210/15
		$p$	$0.190 \pm 0.010$	$1.035 \pm 0.010$	$0.906 \pm 0.016$	$5.899 \pm 0.239$	$14.593 \pm 0.369$	$0.060 \pm 0.008$	15.642/18
		$\pi^-$	$0.104 \pm 0.008$	$1.083 \pm 0.009$	$0.915 \pm 0.015$	$3.507 \pm 0.144$	$12.722 \pm 0.311$	$4.848 \pm 0.540$	26.658/18
		$K^-$	$0.134 \pm 0.009$	$1.071 \pm 0.011$	$0.876 \pm 0.016$	$6.679 \pm 0.248$	$16.198 \pm 0.401$	$0.240 \pm 0.025$	5.850/15
		$\bar{p}$	$0.190 \pm 0.010$	$1.034 \pm 0.010$	$0.906 \pm 0.016$	$5.899 \pm 0.239$	$15.493 \pm 0.371$	$0.048 \pm 0.006$	15.390/18
1(a)	0–20%	$\pi^+$	$0.128 \pm 0.008$	$1.072 \pm 0.009$	$0.922 \pm 0.015$	$4.636 \pm 0.148$	$15.228 \pm 0.396$	$15.329 \pm 1.902$	16.614/18
$d$ -Au	200 GeV	$p$	$0.239 \pm 0.009$	$1.007 \pm 0.005$	$0.928 \pm 0.016$	$5.975 \pm 0.188$	$15.365 \pm 0.318$	$0.623 \pm 0.068$	19.790/13*
1(b)	0–20%	$\pi^-$	$0.128 \pm 0.008$	$1.072 \pm 0.009$	$0.922 \pm 0.015$	$4.636 \pm 0.148$	$15.228 \pm 0.396$	$15.329 \pm 1.902$	16.434/18
STAR	40–100%	$\bar{p}$	$0.257 \pm 0.009$	$1.009 \pm 0.005$	$0.938 \pm 0.015$	$5.985 \pm 0.189$	$15.765 \pm 0.304$	$0.389 \pm 0.039$	42.176/16
		$\pi^+$	$0.102 \pm 0.008$	$1.082 \pm 0.009$	$0.918 \pm 0.016$	$3.297 \pm 0.146$	$12.703 \pm 0.288$	$7.448 \pm 0.859$	15.858/18
		$p$	$0.170 \pm 0.009$	$1.028 \pm 0.006$	$0.962 \pm 0.011$	$5.919 \pm 0.192$	$14.993 \pm 0.325$	$0.268 \pm 0.030$	18.052/13*
1(c)	40–100%	$\pi^-$	$0.102 \pm 0.008$	$1.082 \pm 0.009$	$0.918 \pm 0.016$	$3.297 \pm 0.146$	$12.703 \pm 0.288$	$7.575 \pm 0.859$	12.564/18
		$\bar{p}$	$0.185 \pm 0.009$	$1.033 \pm 0.005$	$0.932 \pm 0.012$	$5.619 \pm 0.190$	$16.093 \pm 0.306$	$0.152 \pm 0.019$	30.160/16
		$\pi^+$	$0.118 \pm 0.008$	$1.049 \pm 0.009$	$0.883 \pm 0.012$	$2.205 \pm 0.102$	$10.829 \pm 0.302$	$3.057 \pm 0.353$	20.677/23
2(a)	200 GeV	$K^+$	$0.150 \pm 0.009$	$1.054 \pm 0.011$	$0.921 \pm 0.011$	$3.353 \pm 0.126$	$11.993 \pm 0.326$	$0.174 \pm 0.022$	10.440/18
$pp$ STAR		$p$	$0.186 \pm 0.009$	$1.015 \pm 0.009$	$0.846 \pm 0.013$	$3.462 \pm 0.131$	$12.833 \pm 0.362$	$0.086 \pm 0.012$	23.276/22
		$\pi^-$	$0.118 \pm 0.008$	$1.049 \pm 0.009$	$0.873 \pm 0.012$	$2.185 \pm 0.102$	$10.996 \pm 0.305$	$3.000 \pm 0.362$	26.151/23
		$K^-$	$0.150 \pm 0.009$	$1.055 \pm 0.011$	$0.915 \pm 0.011$	$3.353 \pm 0.126$	$12.873 \pm 0.332$	$0.172 \pm 0.023$	6.408/18
2(b)		$\bar{p}$	$0.186 \pm 0.009$	$1.016 \pm 0.009$	$0.841 \pm 0.013$	$3.678 \pm 0.138$	$13.680 \pm 0.378$	$0.067 \pm 0.010$	34.078/22
3(a)	0–5%	$\pi^\pm$	$0.147 \pm 0.008$	$1.051 \pm 0.012$	$0.680 \pm 0.013$	$1.485 \pm 0.098$	$7.209 \pm 0.288$	$87.650 \pm 8.710$	125.493/45*
$p$ -Pb ALICE	5.02 TeV	$K^\pm$	$0.262 \pm 0.008$	$1.059 \pm 0.011$	$0.938 \pm 0.011$	$3.149 \pm 0.123$	$7.339 \pm 0.298$	$2.787 \pm 0.331$	229.635/45
		$p+\bar{p}$	$0.351 \pm 0.009$	$1.030 \pm 0.009$	$0.905 \pm 0.011$	$3.312 \pm 0.148$	$8.331 \pm 0.315$	$0.729 \pm 0.089$	45.795/43
		$\pi^\pm$	$0.114 \pm 0.008$	$1.028 \pm 0.009$	$0.721 \pm 0.014$	$1.335 \pm 0.104$	$7.282 \pm 0.294$	$12.243 \pm 1.292$	574.028/52
3(b)	80–100%	$K^\pm$	$0.168 \pm 0.008$	$1.047 \pm 0.012$	$0.843 \pm 0.012$	$3.485 \pm 0.126$	$8.942 \pm 0.302$	$0.492 \pm 0.058$	126.180/45
		$p+\bar{p}$	$0.188 \pm 0.009$	$1.035 \pm 0.011$	$0.821 \pm 0.012$	$3.582 \pm 0.139$	$9.581 \pm 0.326$	$0.144 \pm 0.017$	103.888/43
		$\pi^\pm$	$0.118 \pm 0.008$	$1.007 \pm 0.004$	$0.593 \pm 0.006$	$1.239 \pm 0.096$	$7.489 \pm 0.285$	$13.902 \pm 1.119$	192.066/54*
4	2.76 TeV	$K^\pm$	$0.172 \pm 0.009$	$1.050 \pm 0.011$	$0.828 \pm 0.006$	$2.995 \pm 0.102$	$8.818 \pm 0.306$	$0.453 \pm 0.058$	102.960/52
$pp$ ALICE		$p+\bar{p}$	$0.221 \pm 0.009$	$1.015 \pm 0.008$	$0.683 \pm 0.005$	$2.782 \pm 0.108$	$9.546 \pm 0.311$	$0.164 \pm 0.018$	152.048/43

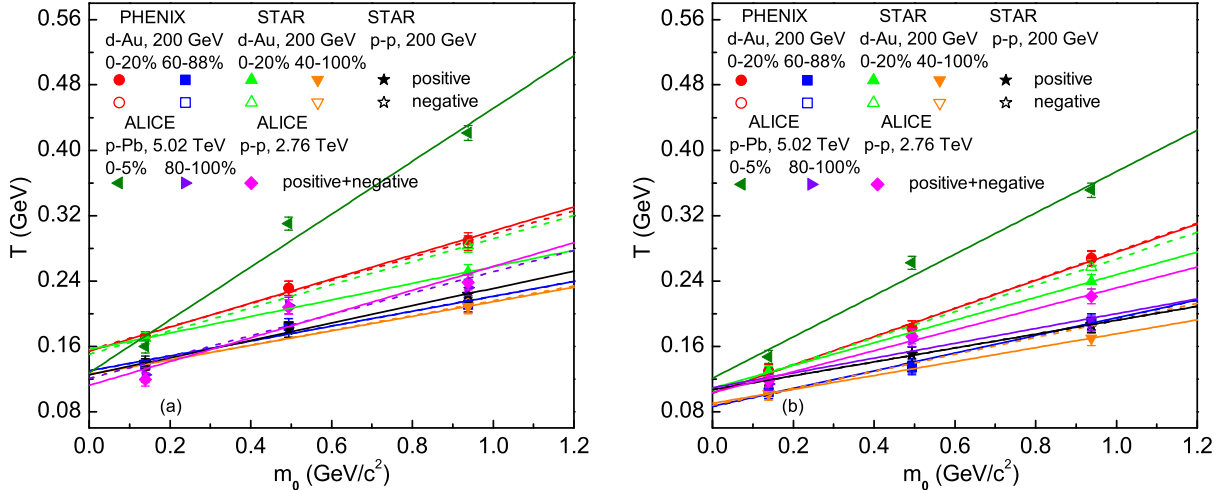


Fig. 5. Relations between  $T$  and  $m_0$ , where panels (a) and (b) correspond to the variants iii) and iv) which use the Boltzmann and Tsallis distributions respectively. The symbols represent values of  $T$  listed in Tables 3 and 4 for different  $m_0$ . The lines are fitted results.

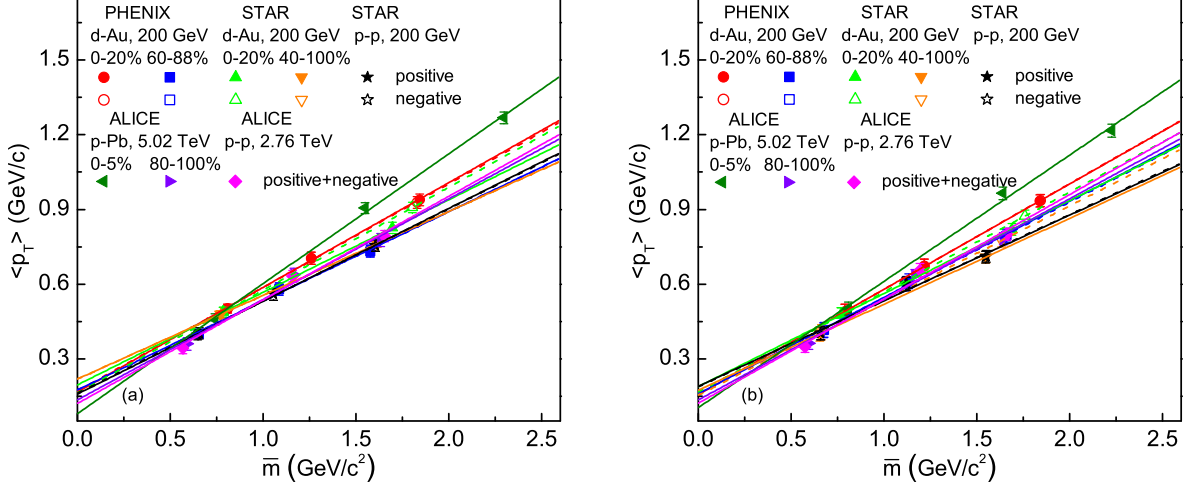


Fig. 6. The same as Fig. 5, but showing the relations between  $\langle p_T \rangle$  and  $\bar{m}$ . The symbols represent values of  $\langle p_T \rangle$  for different  $\bar{m}$ , which are calculated due to the parameters listed in Tables 3 and 4 and the isotropic assumption in the rest frame of emission source.

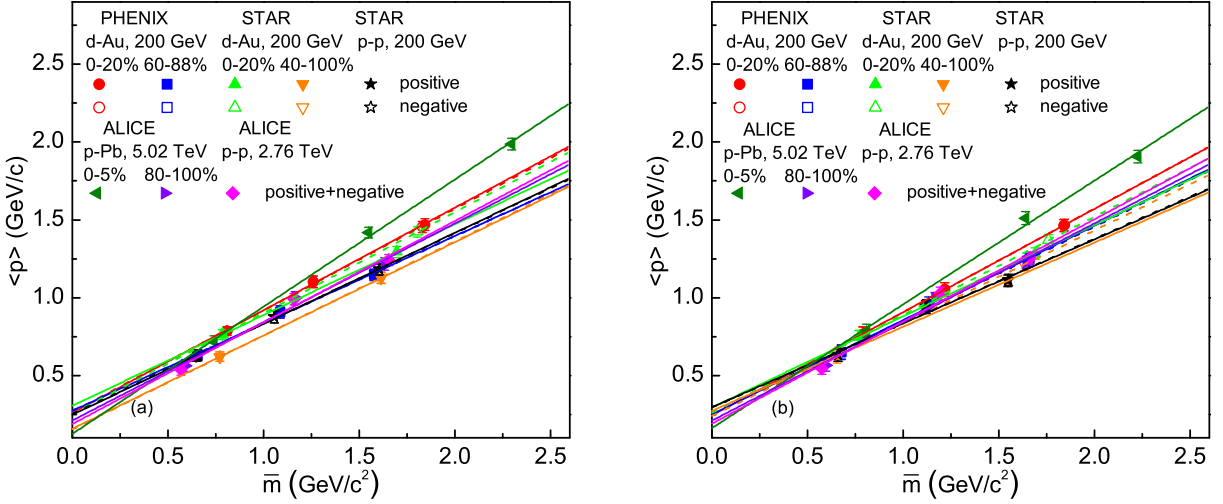


Fig. 7. The same as Fig. 5, but showing the relations between  $\langle p \rangle$  and  $\bar{m}$ . The symbols represent values of  $\langle p \rangle$  for different  $\bar{m}$ , which are calculated due to the parameters listed in Tables 3 and 4 and the isotropic assumption in the rest frame of emission source.

Table 5. Values of parameters (intercept and slope),  $\chi^2$ , and dof corresponding to the linear relations obtained from the fits of the Boltzmann distribution in Figs. 5(a), 6(a), and 7(a).

Figure	Relation	Type	Sign	Centrality	Intercept	Slope	$\chi^2/\text{dof}$
5(a)	$T - m_0$	$d\text{-Au } 200 \text{ GeV}$ PHENIX	+	0–20%	$0.154 \pm 0.006$	$0.147 \pm 0.010$	$0.460/1$
			–	0–20%	$0.155 \pm 0.008$	$0.142 \pm 0.012$	$0.737/1$
			+	60–88%	$0.130 \pm 0.014$	$0.091 \pm 0.022$	$2.378/1$
			–	60–88%	$0.130 \pm 0.014$	$0.091 \pm 0.022$	$2.378/1$
		$d\text{-Au } 200 \text{ GeV}$ STAR	+	0–20%	$0.156 \pm 0.000$	$0.101 \pm 0.000$	$0.000/0$
			–	0–20%	$0.150 \pm 0.000$	$0.141 \pm 0.000$	$0.000/0$
			+	40–100%	$0.126 \pm 0.000$	$0.089 \pm 0.000$	$0.000/0$
			–	40–100%	$0.125 \pm 0.000$	$0.090 \pm 0.000$	$0.000/0$
		$pp \text{ } 200 \text{ GeV}$ STAR	+		$0.125 \pm 0.004$	$0.106 \pm 0.006$	$0.173/1$
			–		$0.127 \pm 0.003$	$0.104 \pm 0.005$	$0.089/1$
		$p\text{-Pb } 5.02 \text{ TeV}$ ALICE	+/-	0–5%	$0.128 \pm 0.030$	$0.324 \pm 0.049$	$11.858/1$
			+/-	80–100%	$0.121 \pm 0.033$	$0.130 \pm 0.054$	$9.817/1$
		$pp \text{ } 2.76 \text{ TeV ALICE}$	+/-		$0.112 \pm 0.032$	$0.1146 \pm 0.052$	$11.352/1$
6(a)	$\langle p_T \rangle - \bar{m}$	$d\text{-Au } 200 \text{ GeV}$ PHENIX	+	0–20%	$0.166 \pm 0.018$	$0.421 \pm 0.013$	$0.182/1$
			–	0–20%	$0.171 \pm 0.021$	$0.416 \pm 0.015$	$0.251/1$
			+	60–88%	$0.175 \pm 0.035$	$0.358 \pm 0.030$	$0.782/1$
			–	60–88%	$0.175 \pm 0.035$	$0.358 \pm 0.030$	$0.782/1$
		$d\text{-Au } 200 \text{ GeV}$ STAR	+	0–20%	$0.195 \pm 0.000$	$0.372 \pm 0.000$	$0.000/0$
			–	0–20%	$0.162 \pm 0.000$	$0.414 \pm 0.000$	$0.000/0$
			+	40–100%	$0.218 \pm 0.000$	$0.337 \pm 0.000$	$0.000/0$
			–	40–100%	$0.218 \pm 0.000$	$0.337 \pm 0.000$	$0.000/0$
		$pp \text{ } 200 \text{ GeV}$ STAR	+		$0.158 \pm 0.013$	$0.373 \pm 0.011$	$0.107/1$
			–		$0.162 \pm 0.011$	$0.371 \pm 0.009$	$0.071/1$
		$p\text{-Pb } 5.02 \text{ TeV}$ ALICE	+/-	0–5%	$0.080 \pm 0.032$	$0.522 \pm 0.019$	$0.904/1$
			+/-	80–100%	$0.135 \pm 0.064$	$0.404 \pm 0.053$	$2.214/1$
		$pp \text{ } 2.76 \text{ TeV ALICE}$	+/-		$0.120 \pm 0.057$	$0.416 \pm 0.047$	$2.379/1$
7(a)	$\langle p \rangle - \bar{m}$	$d\text{-Au } 200 \text{ GeV}$ PHENIX	+	0–5%	$0.260 \pm 0.028$	$0.659 \pm 0.020$	$0.182/1$
			–	0–5%	$0.267 \pm 0.033$	$0.652 \pm 0.024$	$0.251/1$
			+	60–88%	$0.274 \pm 0.055$	$0.561 \pm 0.047$	$0.784/1$
			–	60–88%	$0.274 \pm 0.055$	$0.561 \pm 0.047$	$0.784/1$
		$d\text{-Au } 200 \text{ GeV}$ STAR	+	0–20%	$0.305 \pm 0.000$	$0.583 \pm 0.000$	$0.000/0$
			–	0–20%	$0.254 \pm 0.000$	$0.648 \pm 0.000$	$0.000/0$
			+	40–100%	$0.158 \pm 0.000$	$0.600 \pm 0.000$	$0.000/0$
			–	40–100%	$0.154 \pm 0.000$	$0.604 \pm 0.000$	$0.000/0$
		$pp \text{ } 200 \text{ GeV}$ STAR	+		$0.248 \pm 0.020$	$0.585 \pm 0.017$	$0.106/1$
			–		$0.253 \pm 0.017$	$0.581 \pm 0.014$	$0.070/1$
		$p\text{-Pb } 5.02 \text{ TeV}$ ALICE	+/-	0–5%	$0.125 \pm 0.050$	$0.817 \pm 0.030$	$0.905/1$
			+/-	80–100%	$0.211 \pm 0.100$	$0.633 \pm 0.082$	$2.213/1$
		$pp \text{ } 2.76 \text{ TeV ALICE}$	+/-		$0.188 \pm 0.089$	$0.652 \pm 0.074$	$2.376/1$

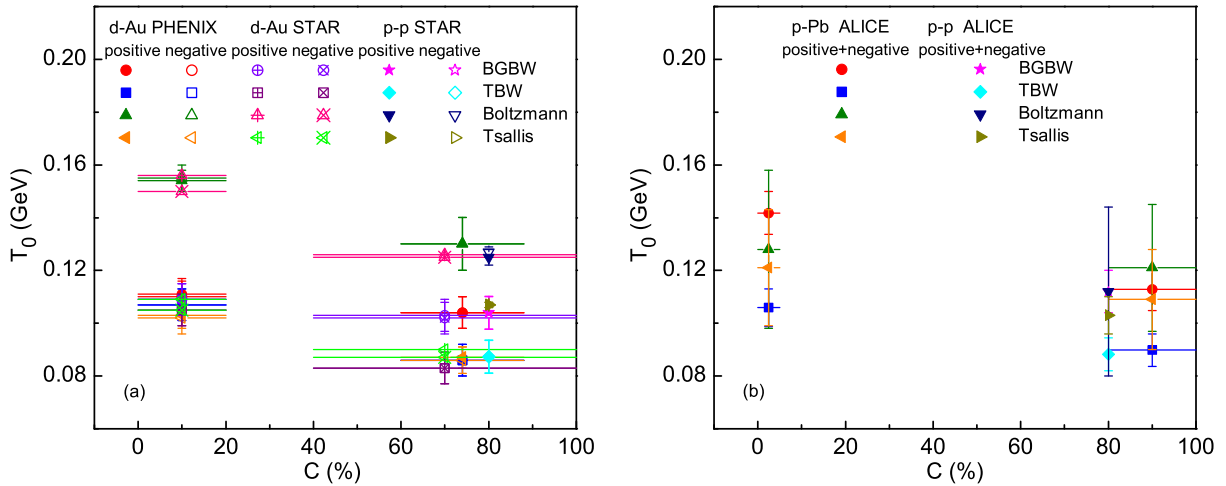


Fig. 8. Dependences of  $T_0$  on  $C$ . Panel (a) corresponds to  $d\text{-Au}$  collisions at  $\sqrt{s_{NN}} = 200 \text{ GeV}$  and  $pp$  collisions at  $\sqrt{s} = 200 \text{ GeV}$ , panel (b) corresponds to  $p\text{-Pb}$  collisions at  $\sqrt{s_{NN}} = 5.02 \text{ TeV}$  and  $pp$  collisions at  $\sqrt{s} = 2.76 \text{ TeV}$ , and the results for  $pp$  collisions are artificially placed at  $C = 80\%$  for comparison. Different symbols represent the results corresponding to different variants and event samples marked in the panels.

Table 6. Values of parameters (intercept and slope),  $\chi^2$ , and dof corresponding to the linear relations obtained from the fits of the Tsallis distribution in Figs. 5(b), 6(b), and 7(b).

Figure	Relation	Type	Sign	Centrality	Intercept	Slope	$\chi^2/\text{dof}$
5(b)	$T - m_0$	$d\text{-Au } 200 \text{ GeV}$ PHENIX	+	0-20%	$0.103 \pm 0.008$	$0.172 \pm 0.013$	0.660/1
			-	0-20%	$0.102 \pm 0.008$	$0.174 \pm 0.013$	0.729/1
			+	60-88%	$0.087 \pm 0.007$	$0.108 \pm 0.012$	0.317/1
			-	60-88%	$0.086 \pm 0.007$	$0.108 \pm 0.012$	0.558/1
		$d\text{-Au } 200 \text{ GeV}$ STAR	+	0-20%	$0.109 \pm 0.000$	$0.139 \pm 0.000$	0.000/0
			-	0-20%	$0.105 \pm 0.000$	$0.162 \pm 0.000$	0.000/0
			+	40-100%	$0.090 \pm 0.000$	$0.085 \pm 0.000$	0.000/0
			-	40-100%	$0.087 \pm 0.000$	$0.104 \pm 0.000$	0.000/0
		$pp \text{ 200 GeV}$ STAR	+		$0.107 \pm 0.002$	$0.085 \pm 0.003$	0.030/1
			-		$0.107 \pm 0.002$	$0.085 \pm 0.003$	0.030/1
		$p\text{-Pb } 5.02 \text{ TeV}$ ALICE	+/-	0-5%	$0.121 \pm 0.022$	$0.253 \pm 0.035$	6.083/1
			+/-	80-100%	$0.109 \pm 0.019$	$0.091 \pm 0.031$	4.531/1
		$pp \text{ 2.76 TeV ALICE}$	+/-		$0.103 \pm 0.007$	$0.128 \pm 0.012$	0.600/1
6(b)	$\langle p_T \rangle - \bar{m}$	$d\text{-Au } 200 \text{ GeV}$ PHENIX	+	0-20%	$0.156 \pm 0.003$	$0.423 \pm 0.002$	0.004/1
			-	0-20%	$0.155 \pm 0.002$	$0.425 \pm 0.002$	0.002/1
			+	60-88%	$0.159 \pm 0.028$	$0.387 \pm 0.023$	0.304/1
			-	60-88%	$0.161 \pm 0.023$	$0.385 \pm 0.019$	0.200/1
		$d\text{-Au } 200 \text{ GeV}$ STAR	+	0-20%	$0.188 \pm 0.000$	$0.374 \pm 0.000$	0.000/0
			-	0-20%	$0.167 \pm 0.000$	$0.402 \pm 0.000$	0.000/0
			+	40-100%	$0.174 \pm 0.000$	$0.345 \pm 0.000$	0.000/0
			-	40-100%	$0.154 \pm 0.000$	$0.380 \pm 0.000$	0.000/0
		$pp \text{ 200 GeV}$ STAR	+		$0.189 \pm 0.060$	$0.344 \pm 0.051$	1.532/1
			-		$0.188 \pm 0.060$	$0.346 \pm 0.052$	1.549/1
		$p\text{-Pb } 5.02 \text{ TeV}$ ALICE	+/-	0-5%	$0.103 \pm 0.059$	$0.508 \pm 0.035$	1.883/1
			+/-	80-100%	$0.134 \pm 0.059$	$0.404 \pm 0.049$	2.305/1
		$pp \text{ 2.76 TeV ALICE}$	+/-		$0.121 \pm 0.065$	$0.419 \pm 0.053$	2.562/1
7(b)	$\langle p \rangle - \bar{m}$	$d\text{-Au } 200 \text{ GeV}$ PHENIX	+	0-5%	$0.244 \pm 0.005$	$0.664 \pm 0.004$	0.004/1
			-	0-5%	$0.242 \pm 0.004$	$0.666 \pm 0.003$	0.002/1
			+	60-88%	$0.250 \pm 0.044$	$0.607 \pm 0.036$	0.303/1
			-	60-88%	$0.252 \pm 0.036$	$0.603 \pm 0.029$	0.200/1
		$d\text{-Au } 200 \text{ GeV}$ STAR	+	0-20%	$0.295 \pm 0.000$	$0.586 \pm 0.000$	0.000/0
			-	0-20%	$0.261 \pm 0.000$	$0.630 \pm 0.000$	0.000/0
			+	40-100%	$0.273 \pm 0.000$	$0.541 \pm 0.000$	0.000/0
			-	40-100%	$0.241 \pm 0.000$	$0.596 \pm 0.000$	0.000/0
		$pp \text{ 200 GeV}$ STAR	+		$0.297 \pm 0.094$	$0.539 \pm 0.081$	1.532/1
			-		$0.295 \pm 0.095$	$0.542 \pm 0.081$	1.552/1
		$p\text{-Pb } 5.02 \text{ TeV}$ ALICE	+/-	0-5%	$0.162 \pm 0.092$	$0.795 \pm 0.055$	1.882/1
			+/-	80-100%	$0.210 \pm 0.093$	$0.634 \pm 0.077$	2.310/1
		$pp \text{ 2.76 TeV ALICE}$	+/-		$0.190 \pm 0.102$	$0.657 \pm 0.083$	2.554/1

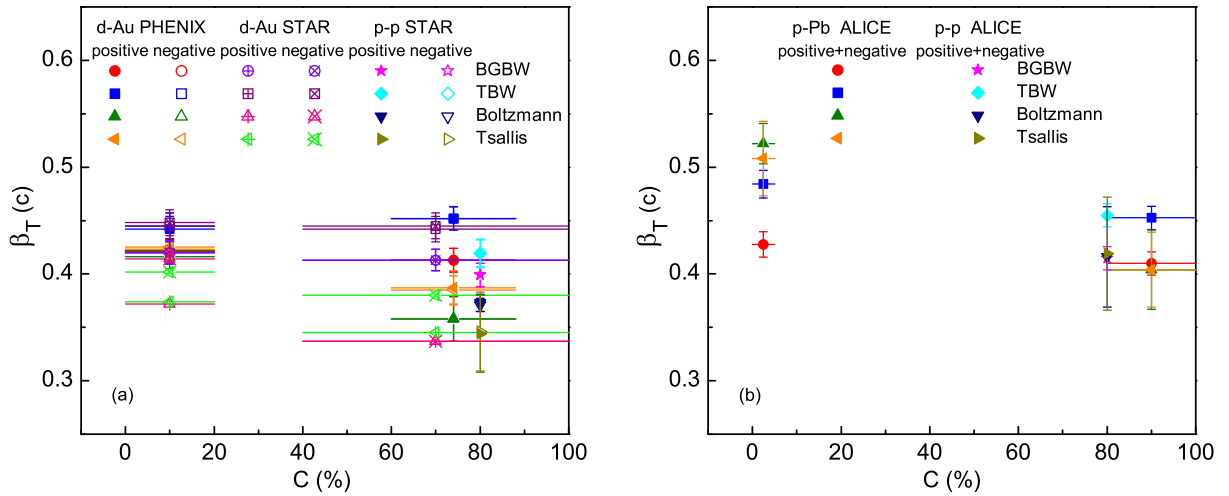


Fig. 9. The same as for Fig. 8, but showing the dependences of  $\beta_T$  on  $C$ .

in the two figures represent overall errors taken from Tables 1, 2, 5, and 6, and different variants result in different errors due to different properties of parameters. In particular, the values of  $T_0$  and  $\beta_T$  in the first two variants are obtained by weighting different particles listed in Tables 1 and 2, and those in the last two variants are obtained by the intercept and slope listed in Tables 5 and 6. One can see that the four variants present similar results, and in some cases these results are in agreement with each other within errors. In central  $d$ -Au and  $p$ -Pb collisions,  $T_0$  is relatively larger than that in peripheral collisions. From the RHIC to LHC energies,  $T_0$  shows a slightly increase or nearly invariant. From peripheral to central collisions and from the RHIC to LHC energies, both  $\beta_T$  show a slightly increase or nearly invariant. These situations are in agreement with our recent work which studied Au-Au collisions at the RHIC and Pb-Pb collisions at the LHC [14]. In particular, the absolute values of  $T_0$  and  $\beta_T$  do not show obvious change from  $d$ -Au ( $p$ -Pb) to Au-Au (Pb-Pb) collisions. In  $pp$  collisions, the dependences of  $T_0$  and  $\beta_T$  on  $\sqrt{s}$  are similar to those in peripheral nucleus-nucleus collisions for not only the changing tendencies but also the values themselves.

In terms of excitation degree which is characterized by  $T_0$ , nucleus-nucleus collisions such as  $d$ -Au, Au-Au,  $p$ -Pb, and Pb-Pb collisions at the RHIC and LHC energies show similar excitation degree at the kinetic freeze-out, though the excitation degree in central collisions is slightly higher than that in peripheral collisions. The excitation degree is dependent of the maximum nucleus, but not the minimum nucleus, in nucleus-nucleus collisions at a given energy. This renders that there is a slightly increase in  $T_0$  with increase of the participant nucleon number in central  $p$ -nucleus collisions when the nucleus is increased in its size. From central  $p$ -nucleus collisions, central  $d$ -nucleus collisions, ..., to central nucleus-nucleus collisions, we can obtain the same or similar excitation degree of the interacting system. This excitation degree is dependent of the maximum nucleus and collision energy, but not the numbers of participant nucleons and binary collisions in central collisions.

As small collision systems,  $pp$ ,  $d$ -Au, and  $p$ -Pb collisions show different features. In terms of  $T_0$  and  $\beta_T$ , comparing with central nucleus-nucleus collisions,  $pp$  collisions are closer to peripheral nucleus-nucleus collisions due to similar numbers of participant nucleons. This is a natural result. Oppositely,  $d$ -Au and  $p$ -Pb collisions are similar to nucleus-nucleus collisions themselves. That is, central  $d$ -Au and  $p$ -Pb collisions are similar to central Au-Au and Pb-Pb collisions, and peripheral  $d$ -Au and  $p$ -Pb collisions are similar to peripheral Au-Au and Pb-Pb collisions, respectively. The small

collision systems,  $pp$ ,  $d$ -Au, and  $p$ -Pb collisions, do not show any new feature in the case of comparing with nucleus-nucleus collisions.

Our recent and present works show some opposite results with the conventional BGBW model which use a less or nearly zero  $\beta_T$  in small collision systems and peripheral nucleus-nucleus collisions [6–8]. The conventional BGBW model results in a less  $T_0$  in central collisions and at the LHC [6–8, 29–34]. In our opinion, because of the entanglement between  $T_0$  and  $\beta_T$ , a less (larger)  $T_0$  can be obtained if a larger (less)  $\beta_T$  is used. Although a nearly zero  $\beta_T$  is used in small collision systems and peripheral nucleus-nucleus collisions by some researchers [6–8], a relatively larger  $\beta_T$  is also used in the mentioned collisions by other researchers using the same BGBW model [7, 35–37]. However, the relatively larger  $\beta_T$  does not change obviously the tendency of  $T_0$ . Only  $T_0$  in central  $d$ -Au collisions is slightly larger than that in peripheral  $d$ -Au collisions at 200 GeV [7]. At the same time, another analysis by using the BGBW model shows that the excitation function of  $T_0$  in central collisions appears a plateau over an energy range from 10 GeV to the LHC [37]. This is not opposite with our result.

Comparing with the conventional BGBW model [6–8, 29–34], other model results are more in agreement with our results. Based on different versions of thermal model, refs. [38, 39] show a slightly larger  $T_0$  in central collisions or an almost invariant  $T_0$  in both central and peripheral collisions. A non-zero  $\beta_T$  in peripheral collisions is used, though  $\beta_T$  in central collisions is still larger than that in peripheral collisions. Based on the TBW model, ref. [9] shows a slightly larger  $T_0$  in central collisions or an almost invariant  $T_0$  in both central and peripheral collisions. A nearly zero  $\beta_T$  in peripheral collisions is used, though  $\beta_T$  in central collisions is very large. Based on different versions of the Tsallis distribution with flow, ref. [40] shows that  $T_0$  extracted from pion spectra in central collisions is less than that in peripheral collisions, and  $T_0$  extracted from kaon or proton spectra does not depend on the centrality. Refs. [41, 42] show that  $T_0$  in central collisions is larger than that in peripheral collisions, and  $T_0$  at the RHIC is less than that at the LHC. For small collision systems and peripheral collisions,  $\beta_T$  is much larger than zero. These situations are in agreement with our results in some cases.

The harmonious results obtained in small system and nucleus-nucleus collisions reveal some universality in hadroproduction process, as it is argued in refs. [43–47]. The universality in hadroproduction process appears in different quantities observed [48] in different types of collisions (including proton-proton, proton-nucleus, and nucleus-nucleus collisions) and/or at different energies

(available from the RHIC even RHIC BES and SPS BES to LHC). These quantities include, but are not limited to, mean multiplicity, rapidity or pseudorapidity density, multiplicity or transverse momentum distribution, and event patterns in different spaces in some conditions. The present work confirms that the universality in hadroproduction process also exists in thermal parameters at the kinetic freeze-out in different types of collisions from the RHIC to LHC [14].

Although the blast-wave model and related distributions themselves lack contributions from resonance decays and strong stopping effects, we can use a two-component form to describe the spectra in very-low and low  $p_T$  ranges. The Tsallis function has connection to thermal model due to its fits to two- or three-component Boltzmann distribution [49]. The index  $q$  represents the degree of non-equilibrium between two or among three states described by Boltzmann distributions, and the Tsallis temperature describes the fluctuations of Boltzmann temperatures. These explanations on the level of drawing curves reveal that the interacting systems at the RHIC and LHC stays in a transition gradation from extensive system to non-extensive system. There is no obvious boundary to distinguish extensive system and non-extensive system for a given interacting system.

Before giving conclusions, we would like to emphasize that the comparisons of different variants and the extractions of  $T_0$  and  $\beta_T$  in small collision system presented in the present work are significative and useful. As discussed above, although many variants or methods are used in literature to extract  $T_0$  and  $\beta_T$  [6–8, 29–42], these variants or methods are hard to give harmonious results in some cases. Indeed, more analyses are needed so that a judgement conclusion can be made. In addition, the hard component has no contribution to  $T_0$  and  $\beta_T$  due to its non-thermal production. Instead, the very-soft and soft components which contribute by the square in the very-low and low  $p_T$  ranges are used to extract  $T_0$  and  $\beta_T$ . So, the third and fourth fits are applicable, because they work for massive particles and in very and low  $p_T$  ranges.

## 4 Conclusions

We summarize here our main observations and conclusions.

(a) The transverse momentum distributions of  $\pi^+$ ,  $\pi^-$ ,  $K^+$ ,  $K^-$ ,  $p$ , and  $\bar{p}$  produced in  $pp$  and  $d$ -Au collisions at the RHIC, as well as  $pp$  and  $p$ -Pb collisions at the LHC, have been analyzed by four variants. The first two variants utilize the blast-wave model with Boltzmann-Gibbs statistics and Tsallis statistics

respectively. The last two variants perform some linear relations in which the Boltzmann and Tsallis distributions are used to extract the effective temperatures respectively. These model and distributions describe only the contribution of soft excitation process. An inverse power-law obtained from the QCD calculus is used to describe the contribution of hard scattering process in the four variants.

(b) The experimental data measured by the PHENIX, STAR, and ALICE Collaborations are fitted by the model results. The four variants present similar results, and in some cases these results are in agreement with each other within errors. Our calculations show that  $T_0$  in central  $d$ -Au and  $p$ -Pb collisions is relatively larger than that in peripheral  $d$ -Au and  $p$ -Pb collisions, and  $\beta_T$  in central  $d$ -Au and  $p$ -Pb collisions is slightly larger than or equal to that in peripheral  $d$ -Au and  $p$ -Pb collisions. With the increase of collision energy from the RHIC to LHC, the considered quantities have slightly increases or they seem to be invariant. These situations are similar to those in Au-Au collisions at the RHIC and Pb-Pb collisions at the LHC for not only the tendencies but also the values of the considered quantities.

(c) The small collision systems such as  $pp$ ,  $d$ -Au, and  $p$ -Pb collisions do not show any particular feature when they are compared with nucleus-nucleus collisions. Comparing with central nucleus-nucleus collisions,  $pp$  collisions are closer to peripheral nucleus-nucleus collisions due to similar numbers of participant nucleons. Central  $d$ -Au and  $p$ -Pb collisions are similar to central Au-Au and Pb-Pb collisions, and peripheral  $d$ -Au and  $p$ -Pb collisions are similar to peripheral Au-Au and Pb-Pb collisions, respectively. In central collisions, the excitation degree at the kinetic freeze-out is mainly determined by the maximum nucleus and collision energy, but not the numbers of participant nucleons and binary collisions.

(d) Combining with our recent work [14], one can see that our results are opposite with the conventional BGBW model due to a large  $\beta_T$  is used by us in peripheral collisions. The conventional BGBW model uses a nearly zero  $\beta_T$  in peripheral collisions and show smaller  $T_0$  in central collisions and at the LHC [6–8, 29–34]. Our results are in agreement with other BGBW [7, 37] or TBW model [9], some thermal models [38, 39], and Tsallis distribution with flow [41, 42]. Ref. [7] shows a slightly larger  $T_0$  in central  $d$ -Au collisions at 200 GeV. Ref. [37] shows the excitation function of  $T_0$  in central collisions appearing a plateau over an energy range from 10 GeV to the LHC. Refs. [9, 38, 39] shows a slightly larger  $T_0$  in central collisions or an almost invariant  $T_0$  in both central and peripheral collisions. Refs. [41, 42] show a larger  $T_0$  in central collisions and

at the LHC. Comparing with  $T_0$ , our results on  $\beta_T$  are more in agreement with other models.

### Conflicts of Interest

The authors declare that there is no conflict of interests regarding the publication of this paper.

### Acknowledgments

This work was supported by the National Natural Science Foundation of China under Grant Nos. 11575103 and 11747319, the Shanxi Provincial Natural Science Foundation under Grant No. 201701D121005, the Fund for Shanxi “1331 Project” Key Subjects Construction, and the US DOE under contract DE-FG02-87ER40331.A008.

## References

- [1] J. Cleymans, H. Oeschler, K. Redlich, and S. Wheaton, Phys. Rev. C **73**, 034905 (2006).
- [2] A. Andronic, P. Braun-Munzinger, and J. Stachel, Nucl. Phys. A **772**, 167 (2006).
- [3] A. Andronic, P. Braun-Munzinger, and J. Stachel, Acta Phys. Pol. B **40**, 1005 (2009).
- [4] A. Andronic, P. Braun-Munzinger, and J. Stachel, Nucl. Phys. A **834**, 237c (2010).
- [5] S. Chatterjee, S. Das, L. Kumar, D. Mishra, B. Mohanty, R. Sahoo, and N. Sharma, Adv. High Energy Phys. **2015**, 349013 (2015).
- [6] E. Schnedermann, J. Sollfrank, and U. Heinz, Phys. Rev. C **48**, 2462 (1993).
- [7] B. I. Abelev et al. (STAR Collaboration), Phys. Rev. C **79**, 034909 (2009).
- [8] B. I. Abelev et al. (STAR Collaboration), Phys. Rev. C **81**, 024911 (2010).
- [9] Z. B. Tang, Y. C. Xu, L. J. Ruan, G. van Buren, F. Q. Wang, and Z. B. Xu, Phys. Rev. C **79**, 051901(R) (2009).
- [10] S. Takeuchi, K. Murase, T. Hirano, P. Huovinen, and Y. Nara, Phys. Rev. C **92**, 044907 (2015).
- [11] H. Heiselberg and A. M. Levy, Phys. Rev. C **59**, 2716 (1999).
- [12] U. W. Heinz, *Lecture Notes for Lectures Presented at the 2nd CERN–Latin-American School of High-Energy Physics*, 1–14 June 2003, San Miguel Regla, Mexico, arXiv:hep-ph/0407360 (2004).
- [13] R. Russo, *Measurement of  $D^+$  meson production in p-Pb collisions with the ALICE detector*, PhD Thesis, Università degli Studi di Torino, Italy, arXiv:1511.04380 [nucl-ex] (2015).
- [14] H.-L. Lao, F.-H. Liu, B.-C. Li, and M.-Y. Duan, arXiv:1703.04944 [nucl-th] (2017).
- [15] H.-R. Wei, F.-H. Liu, and R. A. Lacey, Eur. Phys. J. A **52**, 102 (2016).
- [16] H.-L. Lao, H.-R. Wei, F.-H. Liu, and R. A. Lacey, Eur. Phys. J. A **52**, 203 (2016).
- [17] H.-R. Wei, F.-H. Liu, and R. A. Lacey, J. Phys. G **43**, 125102 (2016).
- [18] J. Cleymans and D. Worku, Eur. Phys. J. A **48**, 160 (2012).
- [19] H. Zheng and L. L. Zhu, Adv. High Energy Phys. **2016**, 9632126 (2016).
- [20] A. Adare et al. (PHENIX Collaboration), Phys. Rev. C **88**, 024906 (2013).
- [21] J. Adams et al. (STAR Collaboration), Phys. Lett. B **637**, 161 (2006).
- [22] G. Agakishiev et al. (STAR Collaboration), Phys. Rev. Lett. **108**, 072302 (2013).
- [23] J. Adams et al. (STAR Collaboration), Phys. Lett. B **616**, 8 (2005).
- [24] J. Adam et al. (ALICE Collaboration), Phys. Lett. B **760**, 720 (2016).
- [25] B. Abelev et al. (ALICE Collaboration), Phys. Lett. B **736**, 196 (2014).
- [26] R. Odorico, Phys. Lett. B **118**, 151 (1982).
- [27] G. Arnison et al. (UA1 Collaboration), Phys. Lett. B **118**, 167 (1982).
- [28] T. Mizoguchi, M. Biyajima, and N. Suzuki, Int. J. Mod. Phys. A **32**, 1750057 (2017).
- [29] S. Das for the STAR Collaboration, EPJ Web of Conf. **90**, 08007 (2015).
- [30] S. Das for the STAR Collaboration, Nucl. Phys. A **904–905**, 891c (2006).
- [31] L. Adamczyk et al. (STAR Collaboration), Phys. Rev. C **96**, 044904 (2017).
- [32] X. F. Luo, Nucl. Phys. A **956**, 75 (2016).
- [33] C. Markert for the STAR Collaboration, J. Phys. G **35**, 044029 (2008).
- [34] I. Melo and B. Tomášik, J. Phys. G **43**, 015102 (2016).
- [35] A. Iordanova for the STAR Collaboration, J. Phys. G **35**, 044008 (2008).
- [36] A. Iordanova for the STAR Collaboration, O. Baranikova, and R. S. Hollis, Int. J. Mod. Phys. E **16**, 1800 (2007).
- [37] A. Ortiz, G. Bencédi, and H. Bello, J. Phys. G **44**, 065001 (2017).
- [38] A. Adler et al. (PHENIX Collaboration), Phys. Rev. C **69**, 034909 (2004).
- [39] S. Chatterjee, B. Mohanty, and R. Singh, Phys. Rev. C **92**, 024917 (2015).
- [40] B. De, Eur. Phys. J. A **50**, 138 (2014).
- [41] D. Thakur, S. Tripathy, P. Garg, R. Sahoo, and J. Cleymans, *Proceedings of the 11th Workshop on Particle Correlations and Femtoscopy (WPCF 2015)*, 3–7 Nov. 2015, Warsaw, Poland, arXiv:1603.04971 [hep-ph] (2016).
- [42] D. Thakur, S. Tripathy, P. Garg, R. Sahoo, and J. Cleymans, Adv. High Energy Phys. **2016**, 4149352 (2016).
- [43] E. K. G. Sarkisyan and A. S. Sakharov, AIP Conf. Proc. **828**, 35 (2006).
- [44] E. K. G. Sarkisyan and A. S. Sakharov, Eur. Phys. J. C **70**, 533 (2010).



- [45] A. N. Mishra, R. Sahoo, E. K. G. Sarkisyan, and A. S. Sakharov, Eur. Phys. J. C **74**, 3147 (2014).
- [46] E. K. G. Sarkisyan, A. N. Mishra, R. Sahoo, and A. S. Sakharov, Phys. Rev. D **93**, 054046 (2016).
- [47] E. K. G. Sarkisyan, A. N. Mishra, R. Sahoo, and A. S. Sakharov, Phys. Rev. D **94**, 011501(R) (2016).
- [48] C. Patrignani et al. (Particle Data Group), Chin. Phys. C **40**, 100001 (2016) and 2017 update.
- [49] F.-H. Liu, Y.-Q. Gao, and B.-C. Li, Eur. Phys. J. A **50**, 123 (2014).